Copyright Undertaking

This thesis is protected by copyright, with all rights reserved.

By reading and using the thesis, the reader understands and agrees to the following terms:

1. The reader will abide by the rules and legal ordinances governing copyright regarding the use of the thesis.
2. The reader will use the thesis for the purpose of research or private study only and not for distribution or further reproduction or any other purpose.
3. The reader agrees to indemnify and hold the University harmless from and against any loss, damage, cost, liability or expenses arising from copyright infringement or unauthorized usage.

If you have reasons to believe that any materials in this thesis are deemed not suitable to be distributed in this form, or a copyright owner having difficulty with the material being included in our database, please contact lbsys@polyu.edu.hk providing details. The Library will look into your claim and consider taking remedial action upon receipt of the written requests.

Pao Yue-kong Library, The Hong Kong Polytechnic University, Hung Hom, Kowloon, Hong Kong

http://www.lib.polyu.edu.hk

FABRICATION AND CHARACTERIZATION OF GALLIUM NITRIDE BASED HETEROJUNCTIONS ETCHED BY PHOTOELECTROCHEMICAL WET ETCHING

By

Gao Jie

SUBMITTED IN PARTIAL FULFILLMENT OF THE REQUIREMENTS FOR
THE DEGREE OF MASTER OF PHILOSOPHY
AT
THE HONG KONG POLYTECHNIC UNIVERSITY
HONG KONG
NOVEMBER 2005

Pao Yue-kong Library
PolyU · Hong Kong

CERTIFICATE OF ORIGINALITY

I hereby declare that this thesis is my own work and that, to the best of my knowledge and belief, it reproduces no material previously published or written, nor material which has been accepted for the award of any other degree or diploma, except where due acknowledgement has been made in the text.

_____________________ (Signature)

GAO Jie (Name of student)

Acknowledgements

There are many people I would like to thank for their contributions to this thesis and many memorable shared experiences throughout my graduate study in Hong Kong Polytechnic University. My first and most heartfelt thank goes to my advisor, Professor Charles Surya. Thank for offering me an opportunity to join Thin Film Optoelectronics Research Group as an M. Phil. candidate, for providing an environment in which I obtain an outstanding technical background and learn to work and think independently, and for his continuous leadership and advice.

A note of gratitude also goes to the members of our group, Dr. C. F. Zhu, Mr. C. W. Lip, Mr. B. H. Leung, Dr. W. K. Fong, Mr. C. P. Chan, Mr. X. F. Lui, Mr. S. K. Jha, and Mr. K. H. Leung, for their helpful discussions, encouragement, and friendship. I am fortunate to have the opportunity to work with these people. I have learned a great deal from them and have greatly enjoyed many days and nights we have worked together. My special thanks go to Dr. C. F. Zhu, Dr. W. K. Fong, Mr. X. F. Lui, Mr. B. H. Leung and Mr. K. H. Leung, for making this thesis possible. I would also like to thank all the collaborators, Miss Q. Tang in Department of Mechanical Engineering, technicians Mr. M. N. Yeung and Mr. C. S. Lo in Department of Applied Physics, and Microelectronics Laboratory in Hong Kong University of Science and Technology.

Finally, I deeply appreciate my parents for all of their understanding, encouragement and care during my study in Hong Kong. And friends continue to be a source of great inspiration to me through the hard times. I'm so proud of having them in my life.

Jie Gao

Hong Kong, China

November, 2005

Table of Contents

Table of Contents ii

List of Figures iv

List of Symbols vi

Abstract viii

Chapter 1. Introduction 1

1.1 Review of Gallium Nitride (GaN) Semiconductor …………………… 1
1.2 Etching of GaN ……………………………………………………… 3
1.3 Motivation and Thesis Overview ……………………………………… 6

Chapter 2. Theory and Characterization of Photoelectrochemical Wet Etching for GaN based Films 10

2.1 Mechanism of Photoelectrochemical Wet Etching …………………… 10
2.1.1 Reaction Mechanism …………………………………………… 10
2.1.2 PEC Wet Etching for Different Doped GaN Thin Films ……… 15
2.2 Characterization Techniques …………………………………………… 18
2.2.1 Etching Rate Characterization ………………………………….. 18
2.2.2 Surface Morphology …………………………………………… 19
2.2.3 Hall Effect Measurement ………………………………………. 24
2.2.4 Low-frequency Noise Theories ………………………………….. 28

Chapter 3. Experiments 34

3.1 Sample Preparation and Fabrication ……………………………………. 34
3.1.1 Growth of GaN and AlGaN/GaN Heterostructure on Sapphire Substrates ……………………………………………………… 34
3.1.2 Sample Preparation …………………………………………….... 35
3.1.3 ICP Dry Etching ……………………………………………….... 36
3.1.4 Cross-bridge Structure Fabrication …………………………….... 37
3.2 Experimental Setup and Approaches for PEC Wet Etching 38
3.2.1 Experimental Equipment ……………………………………….. 38
3.2.2 Experimental Approaches ……………………………………….. 42
3.3 Sample Analyses ……………………………………………………….. 46
3.3.1 Alpha-step Experimental Setup …………………………………... 47
3.3.2 Atomic Force Microscope and Scanning Electron Microscope Experimental Setup ……………………………………………… 47
3.3.3 Hall Measurement Experimental Setup ………………………… 48
3.3.4 Noise Measurement Setup ……………………………………….. 48

Chapter 4. Experimental Results 50
4.1 Results of PEC Wet Etching and Corresponding Characteristics ………. 50
4.1.1 Electrode PEC Wet Etching for n-type GaN …………………….. 50
4.1.2 Electrode PEC Wet Etching for Undoped GaN ………………... 56
4.1.3 Electrodeless PEC Wet Etching for Undoped GaN………………... 58
4.2 Characteristic Analyses of Cross-bridge Structures Fabricated on AlGaN/GaN Heterostructures …………………………………………………………….. 63
4.2.1 Mesa Isolation Obtained by Electrodeless PEC Wet Etching ….. 63
4.2.2 Mesa Isolation Obtained by ICP Wet Etching …………………….. 70

Chapter 5. Discussions 73

Chapter 6. Conclusions and Directions for Future Work 88

Reference 91

List of Figures

1.1 Brief overview of the project

2.1 Experimental apparatus for PEC etching

2.2 Band diagram of the semiconductor/electrolyte interface showing band bending effects on photo-generated electron-hole pairs

2.3 Band diagram of undoped GaN and KOH solution interface

2.4 The basic structure of SEM

2.5 Schematic illustration of the operation of AFM

2.6 Diagram for the inter-molecular force

2.7 AFM feedback loop

2.8 Hall Effect measurement in a cross-bridge structure

3.1 Circular holes pattern on Ti mask

3.2 Cross-bridge structure with the dimension of100μm×30μm

3.3 Cross-bridge structures for Hall Effect and noise measurements

3.4 The whole processes to obtain the mesa structure

3.5 Spectrum of xenon arc lamp

3.6 Electrochemical cell for electrode PEC wet etching

3.7 Detailed flow diagrams of all the steps in PEC wet etching of samples

3.8 The experimental equipment for characterization analyses (a) α-Step 500 Surface Profiler (b) Shield room for low temperature noise measurement (c) Atomic Force Microscope (d) Hall measurement system

3.9 The experimental setup for noise measurement

4.1 Dependences of etching rate on (a) concentration of the solution and (b) light intensity without any bias

4.2 α-Step profile of a typical PEC wet etching with holes as pattern

4.3 Collage of different categories of surface morphology: (a) intermediate smooth etch and dislocation decoration (b) columnar nanostructure (c) nanometer etch pits

4.4 α-Step profile of large area etching in 0.01M KOH

4.5 Etching rates variation with current density

4.6 Undoped GaN sample after PEC wet etching

4.7 Photocurrents for n-type and undoped GaN at the same condition

4.8 Etching rates and RMS roughness of etched surface varied with the concentration of solution at the light intensity of 1.68 W/cm^2

4.9 Etching rates and RMS roughness of etched surface as a function of the light intensity in a 0.1M KOH and 0.05M $K_2S_2O_8$ mixture

4.10 AFM image of the undoped GaN sample

4.11 (a) undoped GaN film etched in 0.1MKOH+0.05M$K_2S_2O_8$ solution. (b) After treatment in 2M KOH solution at 60℃ with ultrasonic for 10 minutes

4.12 SEM micrograph of undoped GaN sample etched with chopped light source

4.13 Hall electron mobility and sheet carrier concentration of the AlGaN/GaN heterostructure versus temperature

4.14 Room temperature Hall mobilities as a function of concentration of the solution and light intensity

4.15 Room temperature voltage noise power densities of cross-bridge devices fabricated with different concentrations of the solution and light intensities

4.16 Experimental $S_V(f)$ measured before (dashed line) and after (solid line) ultrasonic treatment in 2M KOH solution at 60°C

4.17 Temperature dependence of $S_V(f=120\text{Hz})$ for devices H, E and C

4.18 Typical experimental results on $S_V(f)\times f$ for sample C from 120K to 150K

4.19 Hall Mobility varies with temperature for ELPEC and ICP devices

4.20 Room temperature $S_V(f)$ of ELPEC- (triangle) and ICP- (square) etched devices

5.1 Ultrasonic treatments in 2M KOH solution at 60℃ for 10 minutes

5.2 Arrhenius plots of the fluctuation time constant τ

5.3 Low temperature G-R noise magnitude $\log_{10}(S_0)$ is plotted as a function of temperature

5.4 Typical results illustrating the sheet trap density in samples

List of Symbols

A	cross-section area of cross-bridge structure
B_Z	a magnetic field in the z-direction
c	the speed of light
C	a proportionality constant
d	the etched depth
D	the diameter of the hole
E	the thermal activation energy
E_F	Fermi level
E_T	the trap energy
E_y	an electrical potential in the y-direction
f	frequency
f_T	the fraction of traps are filled
g	the trap degeneracy factor
h	the Plank's constant
H	the thickness of the active layer
I	current flow in the sample
ΔI_0	the current fluctuation due to the capture of a single carrier
k	the Boltzmann constant
L	length of cross-bridge structure
m	the mass of solute solid
M	molar mass of GaN
n	the carrier density
n_s	the sheet carrier density
N	total number of the free carriers in the sample
N_A	Avogadro's number
N_T	the trap density
P	the reading power of the light source
q	electronic charge

R	the device resistance
R_H	Hall coefficient
R_{Hs}	a sheet Hall coefficient
R_s	series resistance
S	the etched area of sample
$S_v(f)$	the voltage power spectral density
T	the absolute temperature
v_x	velocity of the charge carriers in the *x*-direction
V	the volume of DI water
V	the voltage drop between the noise measurement contacts
V_h	Hall voltage
V_r	resistance voltage
W	width of cross-bridge structure
x_i	the data collected at every scanning point
X	the number of scanning points for AFM measurement
X_{RMS}	RMS roughness of the scanned area
α	Hooge parameter
λ	wavelength of the light source
ρ	the density of GaN
ρ_s	a sheet resistivity
μ	Hall mobility
Ω	the total volume of the device
τ	the fluctuation time constant
τ_0	the inverse phonon frequency

Abstract

The photoelectrochemical (PEC) wet etching technique was used to etch semi-insulating-GaN epitaxial layers grown by plasma-assisted MBE on sapphire substrates. Systematic studies were conducted to optimize the etching parameters such as the light intensity and concentration of the solution. It is found that the optimal concentration of the etching solution consisted of 0.1M KOH: 0.05M $K_2S_2O_8$ in proportion of 1:1. The film was etched under the illumination of the He-Cd laser at the light intensity of 1.68W/cm^2. This gives etching rate of about 22nm/min and the root-mean squared (RMS) roughness of the etched surface is 17.38nm. Scanning Electron Microscopy (SEM) and Atomic Force Microscopy (AFM) measurement results indicate that the etched surface is comparable with the as-grown GaN films, and can be further improved by the ultrasonic treatment in hot KOH solution.

To investigate the effects of PEC wet etching on the electronic properties of the films, we fabricated cross-bridge $Al_{0.13}Ga_{0.87}N$/GaN heterostructures under the different etching conditions and ultrasonic treatments. The devices were analyzed by the characterization of cross-bridge structures. Results show that the room temperature Hall mobilities and the low-frequency excess noise levels of the devices vary systematically with the light intensity and the concentration of the solution. These results are consistent with the changes of surface roughness. It is found that when the devices were treated by ultrasonic agitation after etching process, the corresponding noise level decreased. A Lorentzian bump originating from the generation-recombination process is observed at low temperature range and its thermal activation energy is about 86.2meV. In addition, it is observed that the low-frequency excess noise of the devices fabricated by optimal PEC etching condition is about half of an order of magnitude lower than that of the devices fabricated by inductively coupled plasma (ICP) dry etching technique. The room temperature Hooge parameter of the device fabricated under the optimal conditions is found to be 2×10^{-3} compared to a value of 9×10^{-3} for the device fabricated by

conventional ICP etching technique. The experimental results demonstrate that PEC wet etching can be effectively utilized as an alternative technique for the fabrication of GaN devices.

Chapter 1. Introduction

1.1 Review of Gallium Nitride (GaN) Semiconductor

GaN is a compound semiconductor with a wide and direct bandgap of 3.4 *eV*. The alloys of GaN with In and Al span a large range of energies from 0.7 *eV* (InN) to 6.2 *eV* (AlN). Therefore the GaN material system holds the immense potential for the development of optical emitters and detectors with spectral responses varying from the deep ultraviolet throughout the visible wavelengths. High-brightness blue and green GaN based light emitting diodes have been commercially available already. These light emitters are expected to show widespread applications in display, high-density optical storage and general lighting. Of the different III-V semiconductors, gallium nitride is one of the most chemically inert materials. Due to the strong chemical bonds in the semiconductor crystal, GaN based devices are for high-temperature, high-power operations and applications under high intensity exposure. A broad application of GaN electronic devices has also been realized, including high electron mobility transistors (HEMTs), heterojunction bipolar transistors (HBTs), Schottky and PIN rectifiers [1].

The availability of a suitable substrate is one of the important factors affecting the film quality. There is no ideal, lattice-matched substrate on which to carry out epitaxial growth of GaN films. The innovative use of low temperature buffer layers in the late 1980s allowed high-quality GaN films to be grown for the first time on sapphire and SiC substrates [2,3]. Shortly after that, Akasaki *et al*. [4] were the first

group to demonstrate the successful growth of p-type GaN films on sapphire substrate by Metal Organic Chemical Vapour Phase Epitaxy (MOVPE), which had been regarded as a major developmental milestone. These newly available GaN materials have sparked a great level of research into GaN crystal growth, processing, and devices. Despite these improvements in crystal quality and the remarkable commercial success of optical emitters fabricated using these materials, it should be noted that defect densities remain quite high (typical dislocation densities are 10^8-$10^{10}/cm^2$). It has been shown that the optical and electrical properties of Ш-nitrides are strongly affected by intrinsic point defects [5]. For this reason, defect studies closely follow any progress in the growth technology of the III-nitrides materials. In recent years, researchers have successfully taken advantage of the Hydride Vapour Phase Epitaxy (HPVE), Metal Organic Chemical Vapour Deposition (MOCVD), and Molecular Beam Epitaxy (MBE) techniques that have greatly improved the quality of films.

To date, sapphire is the most frequently used substrate for GaN epitaxial growth due to its low price, availability of large-area wafers with good crystallinity and stability at high temperature. Its high resistivity renders sapphire particularly suitable for the high-quality growth of AlGaN/GaN heterostructures for device applications. In this research we have used high-quality GaN films that were grown on sapphire substrates by MBE using a novel intermediate temperature buffer layer (ITBL) structure [6]. Using this technique AlGaN/GaN heterostructures with high 2DEG mobility have been successfully grown and tested in our laboratory.

1.2 Etching of GaN

GaN is characterized by its exceptional stability at high temperature and hostile environment. In particularly, GaN is found to be insoluble in conventional acidic or basic solutions. The low chemical reactivity of the Group Ⅲ-nitrides presents a challenge for the etching of GaN thin films. Therefore GaN etching as an important process of device fabrication has been investigated in this research.

Dry etching is the most popular etching technique currently being used. This technique relies on physical processes provided by accelerating energetic ions towards the surface of the material. Therefore, the inert chemical nature of GaN becomes moot. So the dry etching technique for pattern definition of device fabrication process has attracted considerable attention recently, especially for the fabrication of mesa structures where high etching rates, anisotropic profiles, smooth sidewalls, and equivalent rate etching of dissimilar layers are needed [7]. Reactive Ion Etching (RIE) as a widespread traditional dry etching technique is commonly applied to GaN fabrication. Adesida *et al.* were the first group to report GaN etching in RIE systems using $SiCl_4$, $SiCl_4$/Ar, and $SiCl_4/SiF_4$ plasmas [8]. Of all the RIE etching techniques of GaN, chlorine-based plasmas under high ion energy conditions provide the best results. Furthermore, high-density plasma etching techniques, such as Electron Cyclotron Resonance (ECR) plasma, Chemically Assisted Ion Beam Etching (CAIBE), or ICP have shown improved Ⅲ−Ⅴ nitrides etching characteristics as compared with RIE [9-11].

The main disadvantages of dry etching are the damage at the etched surface and sidewall by bombardment of highly energetic ions and the induced influence on the performance of the optical and electrical devices. In addition, the ions will etch both the mask material and the GaN material. So for the etching of thick films, this method becomes impractical due to the need for constant mask replacement [12]. On the other hand, while the ion beam etching technique does not require a mask, the pattern needs to be directly written onto the surface of the material by the ion beam. This method is very time consuming because the beam has to scan over the entire surface while it is constantly being turned on and off to define a pattern.

In contrast to dry etching, wet etching offers a number of distinct advantages that motivate this work. Wet etching requires minimal and inexpensive apparatus when compared with dry etching systems. In addition, wet etching, which proceeds by purely chemical processes, can provide extremely high etch selectivity with respect to local compositional or structural changes in the semiconductor. The most important merit is that it induces less damage in the processes. Although wet chemical etching has normally been used to solve the problems such as surface damage and dopant selection, there is not a simple traditional wet etching process that can be used to obtain smooth etched surface. GaN crystals are difficult to dissolve in acid and alkali solutions [13,14]. Traditional wet etching for GaN materials results in low quality and high defect density in the etched GaN materials [15,16]. Due to the difficulty in traditional wet etching of GaN, PEC wet etching as an improved technique has been investigated in recent years.

Minsky *et al*. first demonstrated the PEC etching of GaN utilizing HeCd laser illumination (325 nm) in a 45 percent KOH (1:3) solution [17]. Following this initial report, several groups have investigated the PEC etching characteristics in a standard electrochemical cell [18-26]. In particular, the Youtsey group gave detailed and comprehensive analyses on PEC wet etching for n-type GaN. Youtsey *et al*. [22-24] demonstrated the first broad-area PEC etching of GaN using Hg arc lamp illumination in KOH solution. Studies on the relationship between the etching rate and the illumination intensity and concentration of the solution have been done. The highest etching rate of 50nm/min was obtained using 0.02 M KOH solution under 40mW/cm^2 intensity illumination. Previous studies show that p-type and undoped GaN samples cannot be etched under normal conditions [19,20,24]. Although J. E. Borton *et al*. [27] demonstrated that etching of the p-type GaN layer can be achieved by applying a positive bias to the surface through a deposited titanium mask, the technique showed, however, large variations in the etching rate of the exposed regions, which made it difficult for large-scale mesa etching.

In contrast with the approach of electrode PEC wet etching that required the physical connection of samples to an external electrochemical cell, using $K_2S_2O_8$ (peroxydisulfate) as the oxidizing agent instead of a cathode in an electrochemical cell was put forward as what is now commonly known as the electrodeless photoelectrochemical (ELPEC) etching. ELPEC etching as an alternative method has played an important role in the etching of GaN materials. The use of $K_2S_2O_8$ in the context of GaN wet etching was first introduced by Bardwell *et al*. [29,30], but led to

a very poor morphology of the etched surface. Afterward H. Maher *et al*. provided a method in which the $K_2S_2O_8$/KOH solution was used to obtain well-controlled etching rates and smooth and high-quality etched surfaces with a minimal degradation in surface roughness [31]. Not long ago, J. M. Hwang *et al*. [28] reported that undoped GaN and p-GaN were successfully etched in a $K_2S_2O_8$/KOH solution with a chopped UV source by ELPEC etching technique, which provided another way for the etching of undoped GaN materials.

1.3 Motivation and Thesis Overview

In recent years, GaN as one kind of semiconductor materials has played an important role in semiconductor applications. GaN-related materials have a great potential for applications of high power and high temperature microwave electronic devices at high frequency. In particular, the two dimensional electron gas (2DEG) at the AlGaN/GaN interface with a wide bandgap, high breakdown electric field, high electron saturation velocity, and large band discontinuity can result in impressive microwave performances. Moreover, the GaN based light emitting devices provide a possibility for next-generation lighting with the emission of white light through the direct band transition, which possesses greater thermal stability under high power operation.

It has been suggested that the etching of GaN based materials is possible using PEC wet etching technique [17-28]. As mentioned above, the studies on PEC wet etching for n-type GaN has been conducted, but much work still needs to be done for the etching of undoped GaN and p-type GaN materials. Notwithstanding the

difficulties of undoped GaN etching by wet etching technique, the great benefits of wet etching in device performance impel further investigations. The present project is to investigate possibilities in the development of PEC wet etching for high-quality undoped AlGaN/GaN heterostructures to realize mesa isolation structure and to characterize the electronic properties of those samples after etching. This etching method can be utilized to fabricate high electron mobility transistors (HEMTs) and heterojunction bipolar transistors (HBTs). The properties of devices can be substantially improved by avoiding the damage caused by dry etching. In our research, we study both electrode and ELPEC wet etching techniques to find a feasible and repeatable recipe for mesa etching and to demonstrate that PEC etching is a damage-reduced process for device fabrication compared to dry etching. In particular, the method to meliorate the etched surface has been studied extensively.

The thesis is organized as follows: Chapter 2 introduces the theoretical mechanism of PEC wet etching and common characterization techniques used for sample analyses. Chapter 3 presents details of the experimental processes including sample preparation and fabrication, and experimental setups under two categories: PEC wet etching and characterization analyses. Chapter 4 shows the experimental results in two main parts. The first part is the results on PEC wet etching for n-type and undoped GaN films. The second part is on the characterizations and comparisons of cross-bridge structures fabricated under the different etching conditions by PEC etching. And then compare the responding characteristics obtained by PEC technique with that attained by ICP technique. The experimental constitution is shown in Figure

1.1. Chapter 5 discusses and analyzes the experimental results. Some special phenomena are also included in this chapter for detailed investigation. Finally, Chapter 6 summarizes the issues presented in the thesis and brings forward the directions for future work.

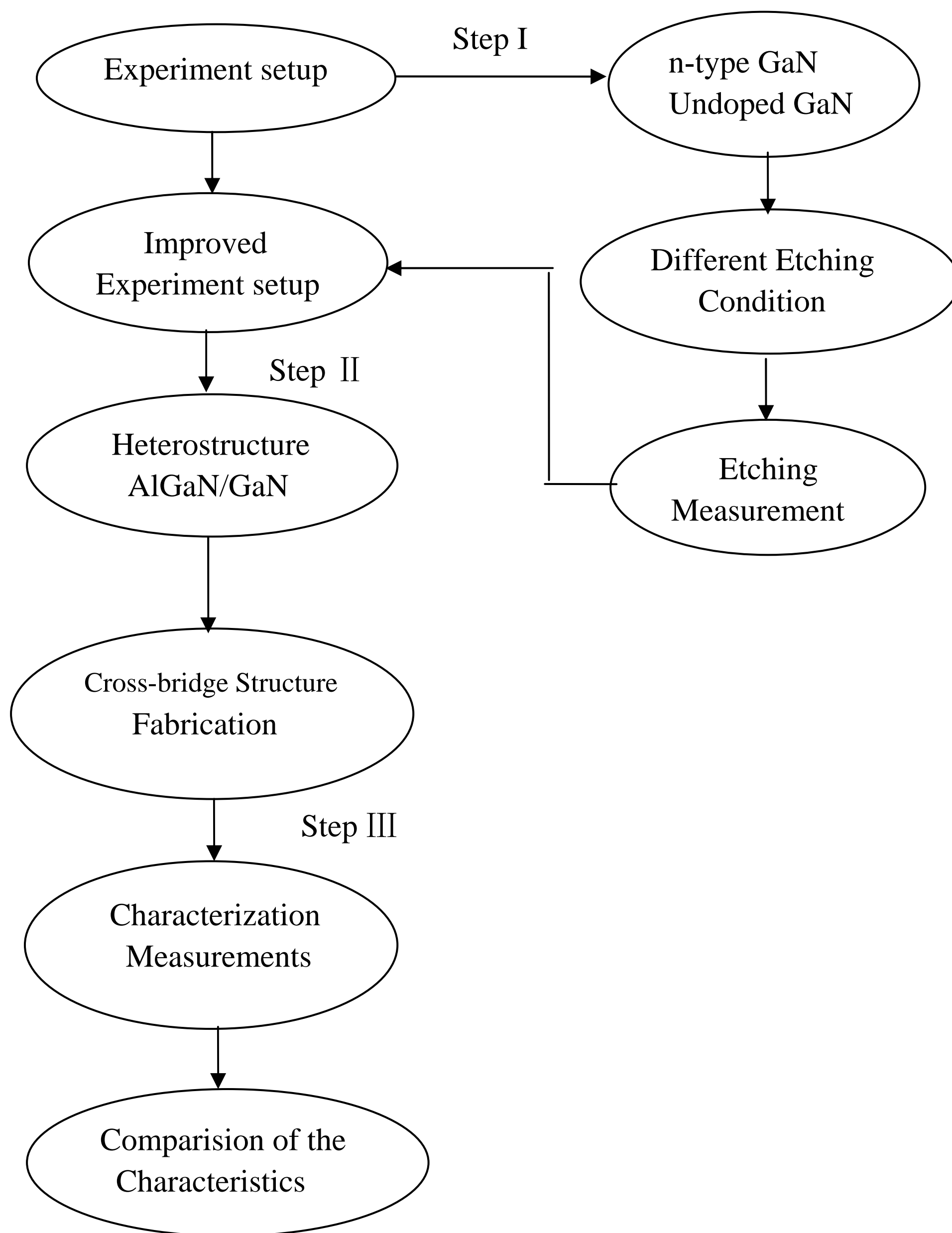

Figure 1.1: Brief overview of the project

Chapter 2. Theory and Characterization of Photoelectrochemical Wet Etching for GaN based Films

2.1 Mechanism of Photoelectrochemical Wet Etching

The procedure of PEC wet etching is affected by many parameters, such as different electrolyte and solution concentrations, the illumination intensity, dopant-type and quality of GaN samples and so on. Thus these parameters encompass a rich variety of etching mechanism, which illustrates a complex range of interactions between the electrolytes, photoinduced carriers at the semiconductor surface, GaN defects and crystal matrixes. At first, the basic theories on electrode and ELPEC wet etching are introduced.

2.1.1 Reaction Mechanism

PEC wet etching technique is shown to be an attractive method to etch GaN in recent years. The etching is enabled by the illumination of the nitride semiconductor surface by photons with greater energy than the bandgap (3.4 *eV* for GaN). The absorbed photons generate electron-hole pairs at the semiconductor surface, which then enhance the electrochemical reaction occurring at the semiconductor/electrolyte interface [32-38]. These electron-hole pairs can result in the dissolution of the GaN. This is the main reason why PEC wet etching is be used for etching GaN, but not "conventional" wet etching. The typical setup used for this process is shown in Figure 2.1. An electrochemical cell consists of the GaN sample as the anode, a Pt cathode

and electrical contact to the semiconductor surface that allows electrons to flow resulting in the acceleration of the redox reactions and etching rates. When connecting an external cathode with the GaN sample in the electrolyte, an electrochemical cell is formed. This is commonly known as the electrode PEC wet etching.

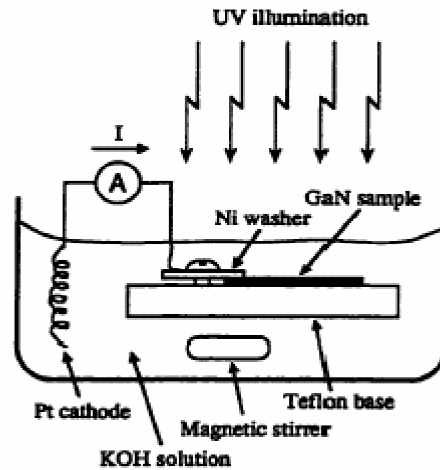

Figure 2.1: Experimental apparatus for PEC etching

The dissolution process of semiconductors by electrolytes is electrochemical in nature and the basic principle of PEC wet etching is redox reactions in a conductive electrolyte. The conventional approach is to form anodic and cathodic areas on the dissolving surface [39]. The illumination of GaN semiconductor surface during etching can result in a high concentration of holes at the surface, and the illuminated regions will become strongly anodic. Cathodic process can occur in the "dark" regions of the surface, or at an external cathode that is electrically connected to the sample if the entire surface of the sample is illuminated (as shown in Figure 2.1), or using a strong oxidant as electrolyte [40]. Since redox reactions couldn't proceed without electrons and holes, PEC wet etching process depends upon the effective

transport of carriers. The electrons and holes created within the space-charge region are transported by 1) migration under the influence of the electric field and 2) diffusion due to a gradient in the carrier concentration. Therefore the transport of carriers is closely related to the dopant-type and conductivity of the semiconductor and the experimental conditions. The detailed transfer process will be discussed later.

Similar to the photo-oxidation of GaAs and other III−V semiconductor materials, there are two steps at GaN anode for PEC wet etching processes: In the first step, GaN is oxidized:

$$2GaN + 6OH^- + 6h^+ \longrightarrow Ga_2O_3 + 3H_2O + N_2 . \qquad (2.1.1)$$

The oxidation reaction can be induced by holes (h^+) in the valence band. In PEC etching, the presence of a hole in the semiconductor at the electrolyte interface is like a broken chemical bond allowing the ionic dissolution of the semiconductor. According to the above reaction, it is clear that the pH value of the electrolyte and the number of holes generated by UV light at the GaN/electrolyte interface have strong influence on the rate of Ga_2O_3 formation. Peng *et al.* [18] proposed that the H_2O solvent plays an important role in the PEC wet etching of GaN. Their experiments showed no PEC wet etching was observed in the solution of KOH dissolved in ethanol. The result suggests that free water molecules play a role in the formation of surface oxides. Subsequently, the oxide layer can be chemically dissolved in KOH solution. It is suggested that the formation of an oxide layer at the GaN/electrolyte interface partially hinders further dissolution of the underlying GaN layer, because the

oxidizing ions have to move across this barrier [41], hence the dissolution of the oxide is an important reaction step in the wet etching process of the GaN material. The reaction governing the dissolution of gallium oxide is

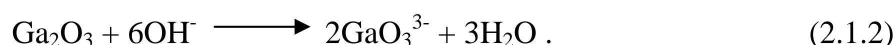

$$Ga_2O_3 + 6OH^- \longrightarrow 2GaO_3^{3-} + 3H_2O \, . \tag{2.1.2}$$

The main factor that brings on the dissolution of gallium oxide is the existence of OH^- ions. The reduction reaction at the Pt cathode proceeds with free water molecules and the electrons from GaN interior:

$$H_2O + e^- \longrightarrow OH^- + H_2 \, . \tag{2.1.3}$$

There are two possible pathways to transport electrons from GaN interior to the electrolyte for the reduction reaction. Figure 2.1 shows that in electrochemical cell, electrons generated in GaN material can be transferred across the semiconductor/ electrolyte interface into the solution to react with water molecules or through the semiconductor/metal interface to Pt cathode by electrical contact between the two electrodes. The motion of electrons induces a photocurrent in the electrochemical cell. How electrons move depends on the reaction kinetics needed for overcoming the barriers in interface. The direction of photocurrent can be determined directly by connecting an ampere meter between the two electrodes.

ELPEC wet etching is another method that differs from the approach described above. The $K_2S_2O_8$ as the oxidizing agent in ELPEC etching replaces the cathode in the electrochemical cell. This approach eliminates the need for a physical connection

between the sample and the cathode. Also, this technique avoids the potential gradient along the distance from the Pt electrode to the GaN film, which may lead to non-uniformity in the etching. The disadvantage is that external biasing cannot be applied to increase the etching rate in the experiment. The carrier transport during the ELPEC etching is similar to that in an electrochemical cell under the open-circuit condition. The basic principles of ELPEC etching are:

i.) oxidation reactions – the same as shown above in electrochemical cell, Eq. (2.1.1) and (2.1.2);

ii.) reduction reactions – $S_2O_8^{2-}$ ions can react electrochemically with conduction-band electrons, creating $SO_4^{-}\bullet$ radical ions. The $SO_4^{-}\bullet$ radical ion is a very strong oxidizing agent and can extract an electron from the valence band of the semiconductor, generating a hole:

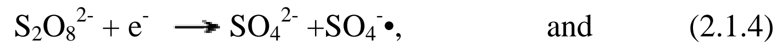

$$S_2O_8^{2-} + e^- \rightarrow SO_4^{2-} + SO_4^{-}\bullet, \quad \text{and} \qquad (2.1.4)$$

$$SO_4^{-}\bullet \rightarrow SO_4^{2-} + h^+. \qquad (2.1.5)$$

Based on the above description of the mechanisms for electrode and electrodeless PEC etching processes, it is clear that the etching process is dependent on a number of parameters as listed below.

1. Light intensity – The rate of etching depends on the rate of photo-generation of the electron-hole pairs. In theory, a linear relationship exists between the etching rate and the light intensity.

2. Solution concentration – As a chemical technique, the concentration of each reagent influences the speed of reactions.
3. Spatial selectivity – By spatial modulation of the light intensity, or by providing the physical masking, one can "anisotropically" etch semiconductors, forming three-dimensional structures. The spatial resolution, which will be discussed for specific cases, is dependent on the semiconductor transport and lifetime properties and on the rate of the chemical reactions.
4. Bandgap selectivity – For materials with different bandgaps, the narrower-gap materials can be selectivity-etched using light with a spectrum that is absorbed by the narrower-gap materials but not by the wider ones.
5. Dopant-type selectivity – Dopant-type of semiconductor influences the band bending that at the semiconductor-electrolyte interface. And this state affects the movement of carriers for chemical reactions. The details will be explained in the next chapter.

2.1.2 PEC Wet Etching for Doped GaN Thin Films

Up to the present, it has been shown that semi-insulating GaN and p-type GaN are very difficult to be etched by PEC wet etching. What is the reason behind this phenomenon? The physical process that underlies the etching of different dopant-type GaN thin films is strongly influenced by the ‘surface band bending’, which depends on the dopant-type and the behavior of photo-generated minority carriers in the near surface region. This is illustrated in Figure 2.2 below:

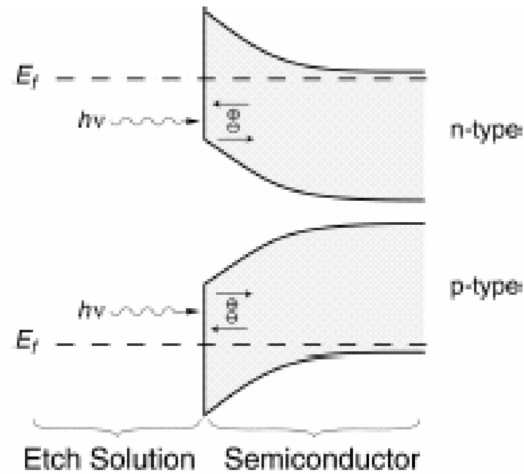

Figure 2.2: Band diagrams of the semiconductor/electrolyte interface show the effects of band bending on photo-generated electron-hole pairs

For n-type materials, a potential well exists for holes at the surface. The opposite situation is found in the case for p-type materials, in which photo-generated holes are swept away from the surface into the bulk. As discussed in the previous sections that excess holes at the surface is essential for the breaking of chemical bonds, making the semiconductor susceptible to the etching solution. Excess electrons at the surface tend to strengthen the bonds, resisting the etching. Only holes generated in the first three or four atomic layers can reach the semiconductor surface by a random, thermal motion, and then play a key role in the oxidation of GaN. The inability to confine photo-generated holes at the semiconductor/electrolyte interface makes p-type samples resistant to etching. The inefficiency of etching undoped GaN is also related to the surface conditions similar to those of p-type GaN materials. Furthermore, the high series resistance of the semi-insulating GaN layer is also a reason for the ineffectiveness of the PEC etching. Recent work has shown that it may be possible to improve the effectiveness of PEC wet etching of undoped GaN and p-GaN materials.

This is the main objective of our project, which is to optimize the process for attaining a mesa structure for high-quality undoped GaN films using wet etching technique with high etching rates. In the following sections, all the possible approaches to increase the etching rates of undoped GaN will be put forward for consideration. The interface of undoped GaN/ KOH solution and charge distribution is shown in Figure 2.3. The Fermi level of undoped GaN semiconductor is nearly at the middle of bandgap [35]. Hence, there is a kinetic barrier for holes to reach the semiconductor/electrolyte interface. In order to etch undoped GaN, one of the main goals is to keep the holes at the reaction interface.

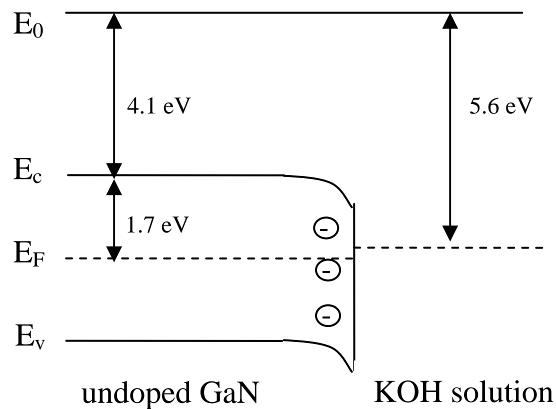

Figure 2.3: Band diagram of undoped GaN and KOH solution interface

2.2 Characterization Techniques

2.2.1 Etching Rate Characterization

For the technology to be applicable in device fabrication, macroscopic-scale etching

has to be realized within a technically reasonable period. The etching rate, determined by measuring the depth of material removed in a given time, represents the average dissolution rate of the semiconductor over the time interval. It should be noted that because of variations in the surface features of the samples, highly precise etching rate measurements are difficult to obtain. Nevertheless, the information is sufficient for observing trends, which may be helpful for the optimization of the process parameters. In addition, when an electrical connection to the sample is made, measuring the current flow in the external circuit can monitor the etching rate. The photocurrent conducted between the GaN sample and the cathode during etching is directly proportional to the instantaneous reaction rate at the semiconductor surfaces by Faraday's law of electrolysis. The relationship between the electrochemical reaction and the GaN mass dissolved in solution has been studied [42]. The etched GaN mass is measured by computing the volume of the material being etched away (sample area × etching depth) multiplied by the density of GaN (ρ=6.095g/cm^3). The number of charges required to remove a given number of Ga and N atoms from the semiconductor surface is determined by the valency of the electrochemical reactions. On the basis of redox reaction Eq. (2.1.1) and Eq. (2.1.2), three electrons are required to remove a single pair of Ga and N atoms. All the electrons needed to remove certain mass of GaN are calculated as

$$Q = \frac{\rho S d}{M} \times N_A \times 3q, \qquad (2.2.1)$$

where S is the etched area of sample, d is the etched depth, M is molar mass of GaN,

N_A is Avogadro's number, q (1.602 x 10^{-19} C) is electronic charge. As photocurrent = Q/t (t is etching time), the actual number of electrons (holes) consumed during the etching process is found by integrating the photocurrent.

2.2.2 Surface Morphology

The surface property will determine how well the material behaves in its intended function. It is therefore vital to characterize the morphology of the films. By far the most important information on surface structure, at least in the first stage of examination of a sample, comes from the techniques that provide images of the structural differentiation in the surface layers [43,44]. In our experiments, we systematically characterized the morphology of the etched surface, in particular the root-mean squared (RMS) roughness, as a function of the etching parameters. This is used as the means to optimize the etching conditions. Scanning Electron Microscopy (SEM) and Atomic Force Microscopy (AFM) techniques are applied for the surface studies.

The simplest and most accessible of all these surface analysis techniques is the SEM. The basic structure of a scanning electron microscope is shown in Figure 2.4 [45]. After the sample is prepared, it is placed in the vacuum chamber. The electron gun at the top produces a beam of monochromatic electrons. The beam is condensed by the first condenser lens. This lens is used to form the beam and limit the amount of current in the beam. It works in conjunction with the condenser aperture to eliminate the high-angle electrons from the beam. The second condenser lens forms the

electrons into a thin, tight, coherent beam. A user selectable objective aperture further eliminates high-angle electrons from the beam. Then a set of coils “scans” or “sweeps” the beam in a grid fashion, dwelling on points for a period of time determined by the scan speed and typically in the microsecond range. The final lens, the objective, focuses the scanning beam onto the part of the specimen desired. When the beam strikes the sample, interactions take place between the electron and the host atoms of the sample and are detected. Before the beam moves to its next dwell point, these instruments count the number of interactions and display a pixel on a CRT whose intensity is determined by this number (the more reactions the brighter the pixel). This process is repeated until the grid scan is finished and then repeated.

SEM is one of the most versatile and widely used tools to investigate the physical morphology of the material. SEM can be divided into two types: conventional SEM and environmental SEM (ESEM). In our case, we have used a conventional SEM to observe non-conductive specimens that are coated with several nanometers of gold. The SEM must always be operated in a vacuum. This is because if the sample is in a gas filled environment, the electron beam cannot be generated or maintained because of a high instability in the beam. Gases will react with the electron source, causing it to burn out. In addition, the electrons in the beam may ionize the gas, which produces random discharges and leads to instability in the beam. A sputter coater operating in high vacuum is also necessary to prepare the sample – coating the sample surface with a layer of gold.

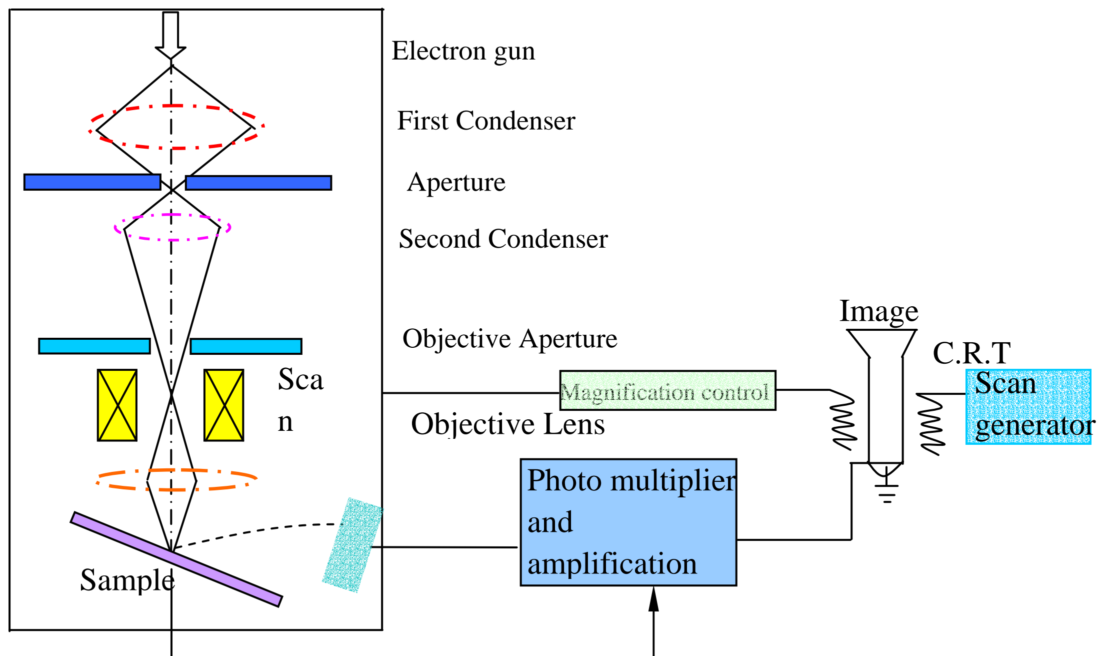

Figure 2.4: The basic structure of SEM

Atomic Force Microscopy (AFM) is another widely used technique for surface analyses. It is designed for qualitative and quantitative measurement of near surface characteristics of the samples with atomic resolution. AFM utilizes a sharp probe moving over the surface of a sample in a raster scan [46,47]. Figure 2.5 shows the schematic illustration of the operation of AFM [48]. A sharp tip mounted on a cantilever is brought to a close proximity of the surface, giving rise to the emergence of a force between the tip and the surface. First the force is attractive, but when the tip-to-sample distance gets very small, on the order of 0.3 nm, the force becomes repulsive and grows very steeply with decreasing distance (Figure 2.6 shows the variation of the force with separation of two atoms [48]). The force acting on the tip will cause the cantilever to deflect. As the cantilever flexes, the light from the laser is

reflected onto the split photo-diode. By measuring the difference signal (A-B), changes in the bending of the cantilever can be measured. Since the cantilever obeys Hooke's Law for small displacements, the interaction force between the tip and the sample can be found. The probe is moved by a piezoelectric bar and thus the tip-surface distance can be obtained. Such scanners are designed to move precisely in any of the three perpendicular axes (x, y, and z). By following a raster pattern, the sensor data forms an image of the probe-surface interaction. Feedback from the sensor is used to maintain the probe at a constant force or distance mode. The AFM feedback loop is shown in Figure 2.7 [46].

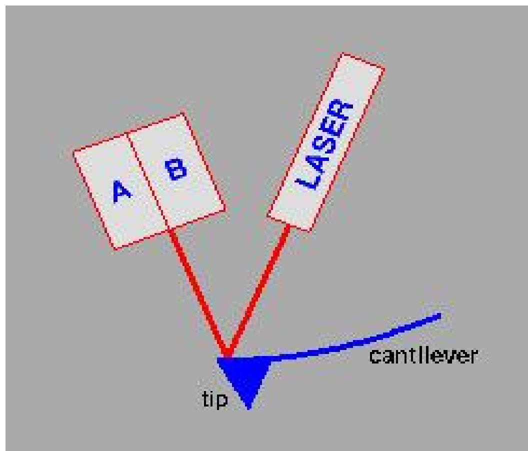

Figure 2.5: Schematic illustration of the operation of AFM

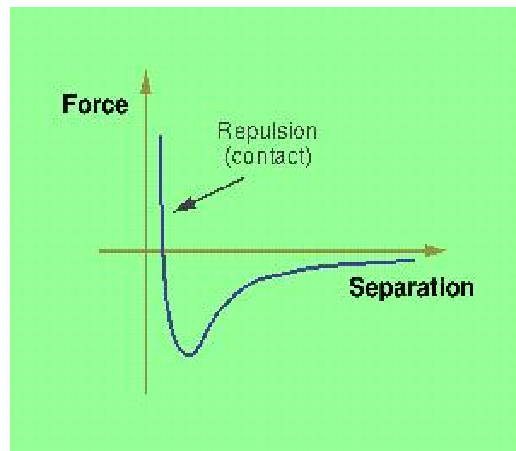

Figure 2.6: Diagram for the inter-molecular force

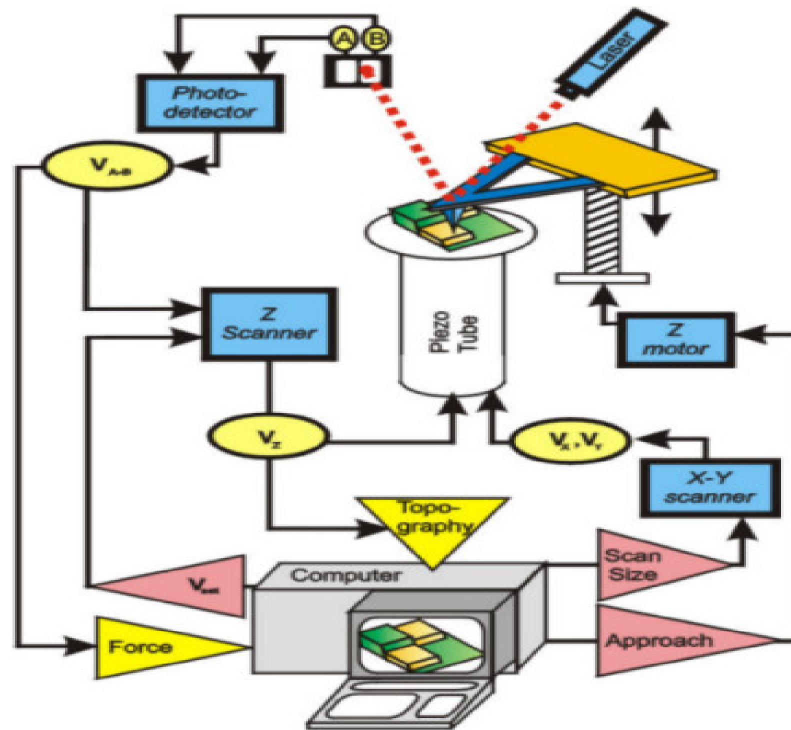

Figure 2.7 AFM feedback loop

AFM can be operated in three regimes: Contact, non-contact and tapping. In our experiments, tapping mode, also known as the semi-contact mode, is selected. The principle of this method will be expounded further in the following sections. When operated in air or other gases, the cantilever oscillates at its resonant frequency (often hundreds of kilohertz) and is positioned above the surface so that it only taps the surface for a very small fraction of its oscillation period. The cantilever is still in contact with the sample, but the very short time over which this contact occurs means that lateral forces are dramatically reduced as the tip scans over the surface. This avoids damages caused by contact mode. In constant force mode, the feedback loop is adjusted so that the amplitude of the cantilever oscillation remains nearly constant. This is accomplished by a control circuit that responds instantaneously to changes on the specimen surface. An image can be formed from this signal.

Comparing these two techniques, the advantage of AFM lies in its ability to image non-conducting surfaces without coating, and the sample is measured in atmospheric pressure as opposed to high vacuum in the case of SEM. In addition, the analysis software in the AFM system provides a tool to evaluate the RMS roughness of the scanned area as a standard parameter for the surface roughness. RMS roughness is a statistical measure of the magnitude of a varying quantity. It can be calculated for a series of discrete values or for a continuously varying function [49]. In the case of AFM, the RMS roughness for a collection of X values $\{x_1, x_2, ..., x_N\}$ is given by the equation below:

$$X_{RMS} = \sqrt{\frac{1}{X}\sum_{i=1}^{X} x_i^2} \quad , \qquad (2.2.2)$$

where X is the number of scanning points set in the software, x_i is the data collected at every scanning point. However, SEM technique is indispensable for surface morphology measurement because it can obtain cross-section images of the specimen from different angles without incision over a large area, which cannot be realized by AFM.

2.2.3 Hall Effect Measurement

Hall Effect measurement is applied as a means for characterizing the transport properties of charged carriers in the 2DEG of a semiconductor heterojunction. It enables one to determine the pertinent information in the material, such as the type, concentration and mobility of the carriers. In general, the carrier density increases

with temperature, and the scattering time, due to lattice scattering, decreases with temperature [50-53]. For highly doped semiconductors, ionized donors or acceptors affect the amount of scattering. In this case, there exist two types of scattering in the semiconductor – lattice scattering and impurity scattering. Impurity scattering is typically more prominent at low temperature.

To measure the Hall voltage from a semiconductor material, a cross-bridge structure is used as shown in Figure 2.8. The basic physical principle underlying the Hall Effect is the Lorentz Force. When an electron moves along the direction (-x) perpendicular to the applied magnetic field B (-z), it experiences a force (-y) acting perpendicular to both directions and causes the electrons to move in response to this force [54-56]. This results in an electric field in a direction perpendicular to the electric current as indicated by E in Figure 2.8, which is the origin of the Hall voltage.

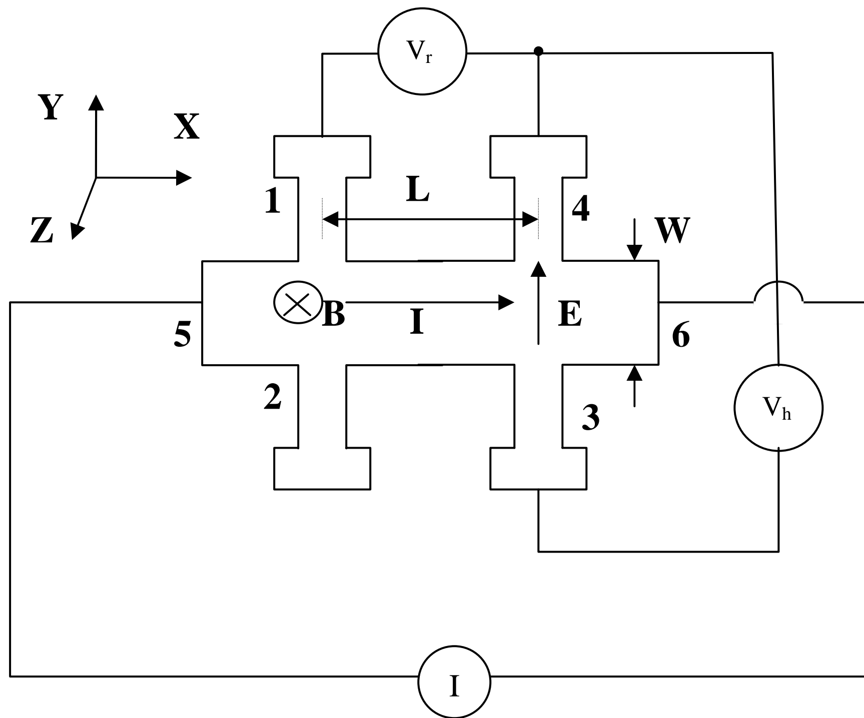

Figure 2.8: Hall Effect measurement in a cross-bridge structure

For an n-type semiconductor the Lorentz force due to the applied magnetic field is given by

$$qE_y = qv_x B_Z , \quad (2.2.3)$$

where q is the electronic charge. The sign of the Hall voltage can be used to determine the doping type of the sample. In the case as described, if V_h is positive (negative), the sample is n-type (p-type).

When a current I flows from contact 5 to contact 6, the resistance voltage V_r is measured between contacts 1 and 4. From the definition of resistance and Ohm's Law, a sheet resistivity ρ_s is given by

$$\rho_s = \frac{\rho}{H} = \frac{R\frac{A}{L}}{H} = \frac{V_r}{I}\frac{W}{L} \quad , \tag{2.2.4}$$

where W and L are the dimensions as defined in Figure 2.8 and H is the thickness of the active layer. The density of the charge carriers may be determined using a theoretical model for current and the definition of Hall coefficient R_H:

$$I = qnHWv_x, \qquad \text{and} \tag{2.2.5}$$

$$R_H = \frac{1}{qn} \quad , \tag{2.2.6}$$

where n is the carrier density. Based on Eq. (2.2.3) and (2.2.5), Eq. (2.2.6) one obtains the sheet Hall coefficient as

$$R_{Hs} = \frac{V_h}{IB_Z} \quad . \tag{2.2.7}$$

The sheet carrier density is calculated from R_{Hs} and is defined as

$$n_s = \frac{IB_Z}{qV_h} \quad . \tag{2.2.8}$$

The calculation of Hall mobility μ depends on the values of ρ_s and $R_{H,}$ which is given by

$$\mu = \frac{R_{Hs}}{\rho_s} = \frac{V_h L}{V_r W B_Z} \quad . \tag{2.2.9}$$

Because the Hall voltage may be quite small, the effects that have a vital influence on the value of the voltage should be considered. The more severe problem comes from the large offset voltage caused by non-symmetric contact placement and

sometimes nonuniform temperature. The most common way to solve this problem is to acquire four sets of Hall measurements at different current directions and two magnetic field directions [54-55]. Therefore the actual V_r and V_h can be expressed as:

$$V_r = {|V_r(I) - V_r(-I)|}/{2} \quad , \qquad \text{and} \qquad (2.2.10)$$

$$V_h = \frac{\left| {|V_h(I)(B) - V_h(-I)(B)|}/{2} + {|V_h(I)(-B) - V_h(-I)(-B)|}/{2} \right|}{2} \quad . \qquad (2.2.11)$$

2.2.4 Low-Frequency Noise Models

Low-frequency noise measurement has been a convenient and nondestructive method to characterize the reliability and lifetime of semiconductor devices. The level of low-frequency noise is not only an important figure-of-merit for the device operating as an amplifier, and also a powerful diagnostic tool of the concentration of defect states in the device [57-62]. One of the most important features of noise characterization is that it allows one to conduct the measurement directly on the device itself. Hence it is a convenient tool for the characterization of the defect states in the active region of the device. Low-frequency noise in semiconductors is classified into four categories: thermal noise, shot noise, *1/f* noise and generation-recombination (G-R) noise. Thermal noise exists in every device, which is caused by the random thermally induced motion of conduction electrons. Shot noise

arises from the motion of the electrons and the discreteness of the electronic charge. Low-frequency excess noises, like *1/f* noise and G-R noise, can be generated as a result of fluctuations in both the number of charge carriers and mobility resulting from the random capture and emission of carriers by traps associated with crystal imperfections, particularly at the crystal surface. This type of noise is significant only at low frequencies. In this thesis, we focus on the study of low-frequency excess noise.

Flicker noise, also known as *1/f* noise, is a universal phenomenon that arises from the capture and emission of free carriers by localized states in the materials. Often the spectral density of *1/f* noise follows a power-law spectrum S, in which $S \propto 1/f^{\gamma}$, where γ is close to unity over the entire observable frequency domain and ranges from 0.8 to 1.4 [57]. The origin of *1/f* noise has been controversial. There are a number of theories for the origin of *1/f* noise, such as Hooge's model, quantum *1/f* noise model, McWhorter's model and thermal activation model.

We first expatiate on the theory of Hooge's model. Hooge parameter has been one commonly used parameter for judging the level of low-frequency excess noise. Hooge *et al*. [63] proposed a phenomenological formula for *1/f* noise:

$$\alpha = \frac{S_V(f)}{V^2} fN \quad , \tag{2.2.12}$$

where the constant α is commonly known as the Hooge parameter, N is the total number of the free carriers in the sample (determined as the value of the sheet carrier

density times the sample area), f is the frequency, $S_V(f)$ is the voltage noise power spectral density at frequency f and V is the dc voltage drop between the noise measurement contacts. It has been pointed out by Handel [64] that a current carried by a beam of electrons and scattered from an arbitrary potential barrier exhibits fluctuations with a *1/f* noise spectrum. This scattering process in a specific semiconductor material with perfect crystalline structure can be identified with a characteristic *1/f* noise coefficient, Hooge parameter. However, Eq. (2.2.12) implies that the noise is dependent on the number of free carriers, and thus a bulk effect. Although some experimental data shows that the relationship mentioned by Hooge is neither exact nor universal, the Hooge relationship cannot be undervalued. It is the only relationship that allows one to estimate the magnitude of the spectral density of *1/f* noise in uniform conductors with an accuracy that most often is no poorer than one or two orders of magnitude [61].

In particular, when traps with discrete energy levels are present in high concentrations, the back ground *1/f* noise may be overwhelmed by the G-R noise [62]. Traps in semiconductors are capable of capturing free electrons (holes) from the conduction (valence) band, and subsequently releasing them, thereby causing perturbation in the carrier concentration and in the flow of current. Possible candidates of traps include shallow and deep levels of donors and acceptors, unintentional impurities in semiconductors, structural defects at crystal surfaces and grain boundaries, threading dislocation, etc [57]. The power spectrum is in the form of a Lorentzian as shown in the following equation by Mc Whoter's Model, [65]

$$S_V(f) = 4N_T\Omega(\Delta I_0)^2 R^2 f_T(1-f_T)\frac{\tau}{1+4\pi^2 f^2\tau^2}$$

$$= S_0 \frac{\tau}{1+4\pi^2 f^2\tau^2} \quad , \tag{2.2.13}$$

where N_T is the trap density, Ω is the total volume of the device, ΔI_0 is the current fluctuation due to the capture of a single carrier, R is the device resistance, τ is the fluctuation time constant, and f_T is the Fermi Dirac distribution function. The trapping and detrapping process is shown to be thermally activated in which τ is given by

$$\tau = \tau_0 \exp\left(-\frac{E}{kT}\right) \ , \tag{2.2.14}$$

where E is the thermal activation energy for the capture and emission of the carriers, k is the Boltzmann constant, T is the absolute temperature and τ_0 is the inverse phonon frequency. The Fermi-Dirac distribution function, f_T, is given by

$$f_T = \frac{1}{1+g\exp(\frac{E_T-E_F}{kT})} \quad , \tag{2.2.15}$$

where E_T is the trap energy, E_F is Fermi level, and g is the trap degeneracy factor. In the case where the noise is dominated by number fluctuation, $S_V(f)$ can be expressed as [66]

$$S_V(f) \approx S_{Vn}(f) = \frac{V^2}{N^2} 4N_T A f_T(1-f_T)\frac{\tau}{1+4\pi^2 f^2\tau^2} \quad , \quad \text{and} \tag{2.2.16}$$

$$S_0(f) = \frac{V^2}{N^2} 4N_T A f_T(1-f_T) \ , \tag{2.2.17}$$

where V is the dc voltage bias applied to the device and N is the number of carriers in the device, A is the sample cross-section area. The cut-off frequencies, given by $1/\tau$, are strongly temperature dependent. When the temperature is lowered, the activation energy of the G-R noise can be evaluated through the Arrhenius plot of the cut-off frequency.

Similar to Mc Whoter's model, the Thermal Activation model for flicker noise states that the fluctuation is caused by the random capture and emission of the carriers by localized states via a thermally activated process. However, in this case the traps are widely distributed in energy rather than concentrating in a single energy level as in the case of the G-R noise. Hence $S_V(f)$ is given by

$$S_V(f) = 4\frac{V^2}{N^2}\int_x \int_y \int_E N_T(x, y, E)\frac{\tau}{1+4\pi^2 f^2 \tau^2} dxdydE . \qquad (2.2.18)$$

Eq. (2.2.18) stipulates that traps at different energy levels all contribute to the overall low-frequency noise and is accounted for through the integral over energy. It is noteworthy that for small activation energy, E, the denominator of the Lorentzian is dominated by the factor "1" and hence the Lorentzian varies as τ and increases exponentially with E. Whereas at high activation energy range, denominator of the Lorentzian is dominated by the factor "$4\pi^2 f^2 \tau^2$" and the Lorentzian varies as "$1/\tau$", which decreases exponentially with the activation energy, E. Thus, Eq. (2.2.18) stipulates that the properties of the low-frequency excess noise is highly sensitive to traps at energy E, where

$$E = -kT\ln\left(2\pi f\tau_0\right) \quad . \tag{2.2.19}$$

This implies that $S_V(f)$, measured at *T*, is a sensitive tool for the characterization of the trap density $N_T(E)$. At a given temperature and frequency, the trap density can be expressed as below:

$$N_T\left(E\right) = \frac{S_V\left(f\right) f N^2}{4V^2 AkT} \, . \tag{2.2.20}$$

Hence one can determine the trap density as function of energy by detailed measurement of the temperature dependence of the low-frequency excess noise.

Chapter 3. Experiments

This chapter describes experimental setup and methods that were developed to carry out PEC wet etching of GaN based materials and the corresponding analyses of the etched samples. In addition, the detailed sample preparation process for the GaN heterostructure used in the etching experiments will be discussed.

3.1 Sample Preparation and Fabrication

3.1.1 Growth of GaN and AlGaN/GaN Heterostructure on Sapphire Substrates

There are three kinds of GaN materials investigated in this project: Silicon-doped GaN (n-type), semi-insulating undoped GaN and AlGaN/GaN heterostructures. The films were all deposited on (0001) sapphire substrates by RF-plasma assisted molecular beam epitaxy (MBE) in our laboratory. A 400Å thick AlN buffer layer, grown at 500℃, was used for all the samples. The n-type GaN films with thickness of about 2μm (electron carrier concentration ~ $10^{17}/cm^3$) were grown at 740ºC. The thickness of undoped GaN layer deposited under 690ºC was about 0.8μm. The AlGaN/GaN heterostructure consists of a 30Å undoped-$Al_{0.13}Ga_{0.87}N$ and a 1μm undoped GaN layer. The AlGaN layer was deposited at 740ºC [6,68].

3.1.2 Sample Preparation

Cross bridge structures were fabricated using materials grown under the conditions as illustrated before. All devices of the same type come from the same epilayer to minimize variations in the film properties.

Before etching, all the samples were first treated in acetone, followed by 2-propanal solvent rinse with an ultrasonic vibration to remove the residual contamination from the surface. This is followed by a rinsing process with de-ionized (DI) water. Finally the samples were blown dry using filtered N_2 gas.

There are two possible types of etching mask used in the experiments: i.) insulating mask, such as wax and SiO_2; and ii.) metal mask, such as Ti and Au layers deposited by e-beam technique. Because the metal mask serves the dual purposes of electric contact and etching mask, it is widely used in PEC wet etching. Moreover it has been shown that semi-insulating materials exhibit enhanced etching only when a metal mask is used in the process. The reason for this is that the mask provides a low-resistance contact for electron flow [32]. In our experiments, we used Ti as the etching mask. The thickness of Ti film was approximately 200 nm and was deposited by electron-beam evaporated technique without annealing following the deposition process. Standard image photolithography was used to pattern Ti and photoresist mask. Ti is easily removed by Buffered Oxide Etchant (BOE) and the photoresist can be dissolved in acetone. For ICP etching, photoresist, AZ 3100 positive resist, is selected as mask without any additional dielectric or metal. The thickness of the

photoresist was about 1.35μm after spin-coating at a rotation speed of 4000 rpm for 20 seconds.

Circular holes with diameter of 4μm and cross-bridge structures of two different sizes are opted in our experiments to investigate the etching characteristics. The sizes of the cross-bridge structures are 100μm×30μm and 110μm×10μm, respectively. The patterns of the circular holes and the cross-bridge structure are illustrated in Figures 3.1 and 3.2 respectively.

Figure 3.1 Circular holes pattern on Ti mask

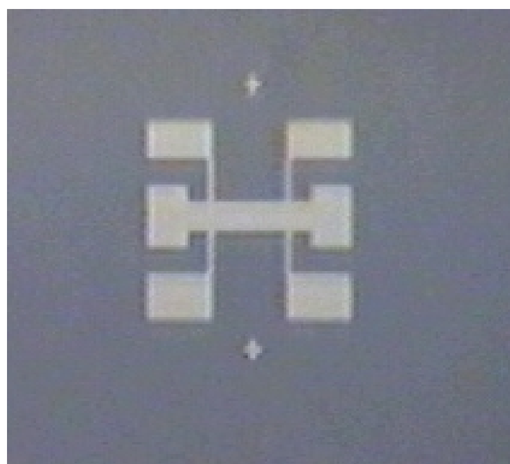

Figure 3.2Cross-bridge structure with the dimension of 100μm×30μm

3.1.3 ICP Dry Etching

ICP dry etching of the GaN samples is performed at the Microelectronics Laboratory, Department of Electrical and Electronic Engineering, Hong Kong University of Science and Technology. The etching condition is the same as that used for LED fabrication in Ref. [69]. In view of the thickness of photoresist, etching lasted 5 minutes and the etching depth was about 600nm.

3.1.4 Cross-bridge Structure Fabrication

Cross-bridge structures isolated by both ICP dry etching and ELPEC wet etching. After the formation of the mesa structures the mask layer were removed by the respective techniques. This is followed by a cleaning process that includes rinsing the devices in acetone, 2-propanal and DI water. Subsequently ohmic contacts for Hall Effect measurement and low-frequency noise measurement were fabricated by e-beam deposition of Ti/Al (60nm/200nm) bilayers and annealing at 810℃ for 30 seconds in a Rapid Thermal Processor (RTP). The contact resistance was measured using transmission line technique and was found to be about 2.5×10^{-4} Ωcm^2. The fabricated samples were placed in an IC package with Al wires ultrasonically bonded to the pads, as shown in Figure 3.3. Well-behaved I-V characteristics for the devices were observed over the entire temperature range of the experiments.

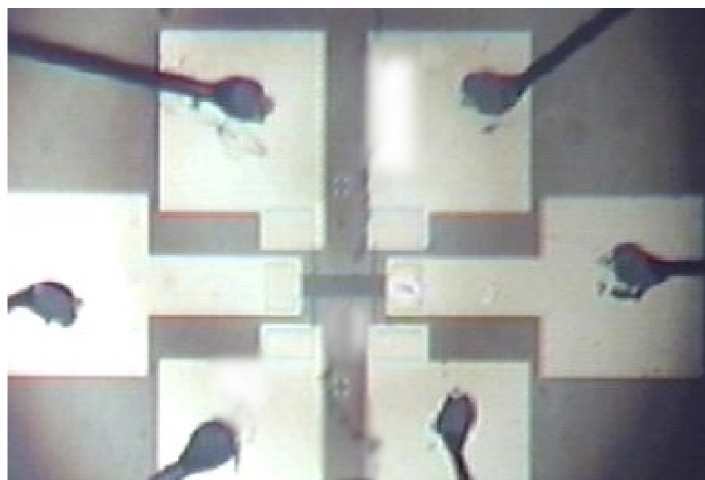

Figure 3.3 Cross-bridge structures for Hall Effect and noise measurements

The whole processes to obtain the mesa structure on AlGaN/GaN heterojunction are shown in Figure 3.4, as below:

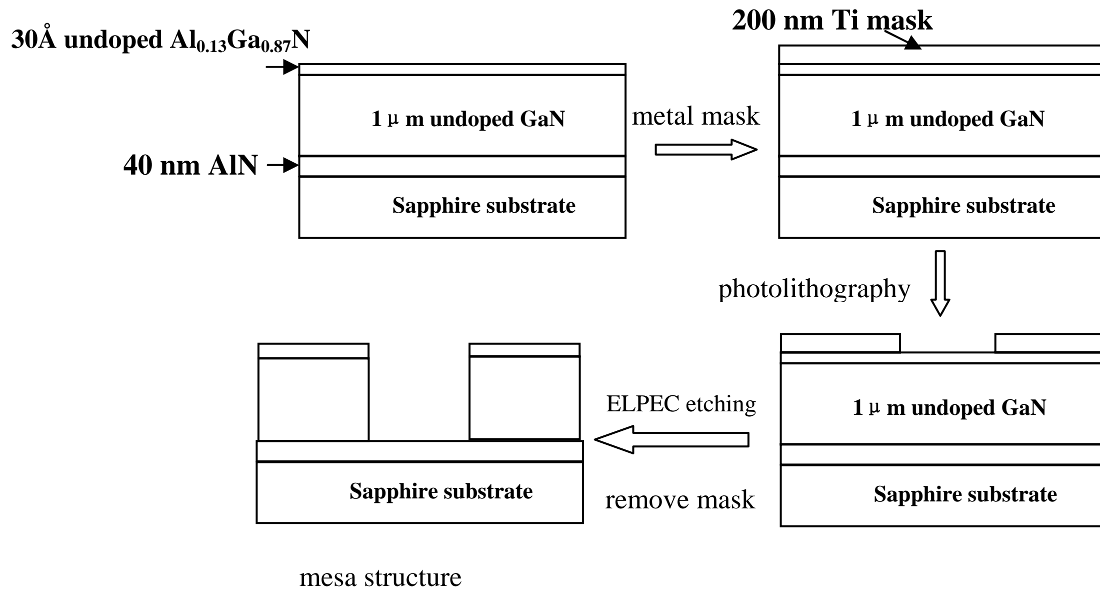

Figure 3.4 The whole processes to obtain the mesa structure

3.2 Experimental Setup and Approaches for PEC Wet Etching

3.2.1 Experimental Equipment

In this section, the hardware developed to carry out PEC wet etching for GaN based materials is discussed.

Ultraviolet light source: In order to produce electron-hole pairs, a light source with energy equal to or greater than the bandgap is used. This energy can be determined from the following equation:

$$E = hc/\lambda \, , \tag{3.2.1}$$

where h is plank's constant, c is the speed of light, and λ is the wavelength of the light. For GaN the calculated wavelength of the light source should be equal to or less than 365 nm. Xenon arc lamp provides broad line output in the UV range can therefore be used to carry out large area fabrication of GaN materials by PEC wet etching. Figure 3.5 shows the spectrum of a xenon arc lamp. The spectrum is continuous in the visible range and extends far into the ultraviolet. A xenon lamp exhibits strong lines in the near infrared between 800 and 1000 nm and some weak lines in the blue portion of the spectrum. Hence it is clear that the illumination intensity of xenon lamp is not strong at 365 nm. Another possible light source is the HeCd laser, which emits a coherent light at 325 nm. In our case, when a high intensity UV radiation is needed, the HeCd laser is the preferential light source. For our experiments, convergent lens or attenuators can be used for modulating the light intensity.

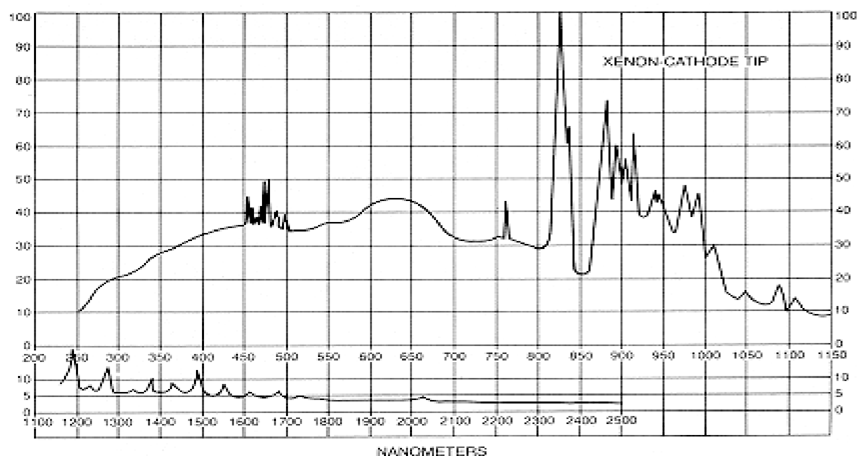

Figure 3.5 Spectrum of xenon arc lamp

Electrolyte: With regard to the selection of electrolyte solution, Peng *et al.* reported GaN can be etched in both aqueous phosphorus acid (H_3PO_4) and potassium

hydroxide (KOH) solution [18]. However, experiments show that using KOH is much more effective for etching GaN films. For ELPEC wet etching, a mixture of $K_2S_2O_8$ and KOH is used. The concentration of the solution can be varied easily by dissolving the appropriate amount of the mixture in DI water, according to the equation below:

$$concentration = m / M \times V , \qquad (3.2.2)$$

where m is the mass of the solute used, M is molar mass of the solute, and V is volume of DI water. The corresponding pH value of the solution can be tested by a pH meter directly.

Light power meter: Illumination intensity is detected by a light power meter. The detector provides the optical power of the light as high as several Watts and wavelength from 250 nm to 800 nm. In order to obtain the normalized value of light intensity, there is a shade with the diameter of 1mm placed before the power meter. The light power induced by the HeCd laser can be directly measured at 325nm by the power meter, and the light intensity can be calculated from

$$\text{light intensity} = 4P / \pi D^2 , \qquad (3.2.3)$$

where P is the reading of the power meter and D is equal to 1mm, the diameter of the hole. Because of the broad spectrum of xenon lamp, the corresponding calculation of light intensity is a little complicated. First the optical power of the lamp at 365nm is first obtained by placing a monochromatic filter after the light source. Then the light intensity at 365nm is calculated. Then the total power from 250nm to 365nm is

evaluated according to the spectral form as shown in Figure 3.4, which is found to be about 100 times that of the power at 365nm. From our calculation it is shown that the maximum light intensity of the xenon lamp in our setup is about 35mW/cm^2.

Sample holder: The main function of sample holder is to fix the sample in the solution. The sample holder is constructed entirely of Teflon due to its inertness to the electrolytes used. Also, being an excellent insulator, the Teflon holder enables good electrical isolation to be achieved. The structure of the holder consists of a platform where the sample can be placed. A Ni washer is used to hold the GaN sample on the Teflon base and Ni is found to be resistant to the attack of KOH electrolyte and it also facilitates electrical contact for electrode PEC etching, in which a current is allowed to flow towards the sample surface to be etched through the Ni washer. Hence, when the Pt counter electrode is electrically connected to the Ni washer, a reduction reaction occurs entirely at the Pt cathode, and not at the Ni washer [70].

Magnetic stirrer: The electrolyte is stirred magnetically to keep the liquid flowing over the sample surface. It is important to stir the solution to keep the bubbles from adsorbing on the etching surface, which will lead to the suppression of the reaction at the sample/electrolyte interface. Also, the stirring action ensures a constant concentration of the electrolyte at the etching surface. It was demonstrated that stirring of the solution during etching maintained the linear relation between light intensity and etching rate. The unstirred solution typically exhibits saturation in the etching rate at higher light intensities [19]. In addition, magnetic stirrer also can help

dissipate the heat produced in the etching process.

Chopper: The function of the chopper in the etching processes has been pointed out by J. M. Hwang *et al*. [28]. In our experiments, we considered improving the experiment results by means of the chopper to engender a periodic UV light pulse during etching. The frequency range of the chopper used in experiments ranges from 4 Hz to 4 kHz with two different sizes of slot blades. In some cases, because the gap between the two adjacent blades is very narrow compared to the magnitude of light spot, it is necessary to use a convergent lens to focus the light in order to decrease the dimension of light spot and to make the sample in the "dark" part of slot blade completely during the "off" cycle.

Besides the above apparatus, some other hardware is used for PEC wet etching. For instance, a constant current source to provide external biasing and an amperemeter to measure the photocurrent between the two electrodes were applied in the process of electrode PEC wet etching.

3.2.2 Experimental Approaches

Figure 3.6 shows the experimental apparatus for electrode PEC wet etching in an electrochemical cell. The light source shined in horizontal direction and was vertically reflected onto the GaN sample surface through the solution using a mirror. The illumination intensity varied with the distance between the sample and the reflector. If necessary, convergent lens or attenuator could be placed between the mirror and the

sample to vary the light intensity for different etching conditions. For electrode PEC wet etching, the platinum cathode and the GaN sample as anode were both wholly immersed in the KOH electrolyte. The solution was agitated with a magnetic stirrer. In our experiments, we found that the depth of the sample into the solution also influenced the etching rates since the solution will absorb the incident UV radiation. If the sample was close to the solution surface, the liquid flowing would be hampered and the etching rate decreased. If the sample was located too far from the surface, the etching rate will also decrease because of the weakened light intensity at the sample surface. So the samples were always placed 1cm below the solution surface. In order to allow effective circulation of the electrolyte, the specimen was fixed in the middle of the beaker. It has been shown that illumining the Pt cathode during the etching process with UV light causes an increase in the etching rate [28]. The reason is that UV photons induce excited electrons (photo-electrons) from the Pt metal which are involved in reduction reaction. Therefore both electrodes were irradiated by the light source during the experimental process. To study the effect of external power supply, a DC constant current source was applied in the external circuit, and a digital multimeter was used to measure the magnitude and the direction of the photocurrent.

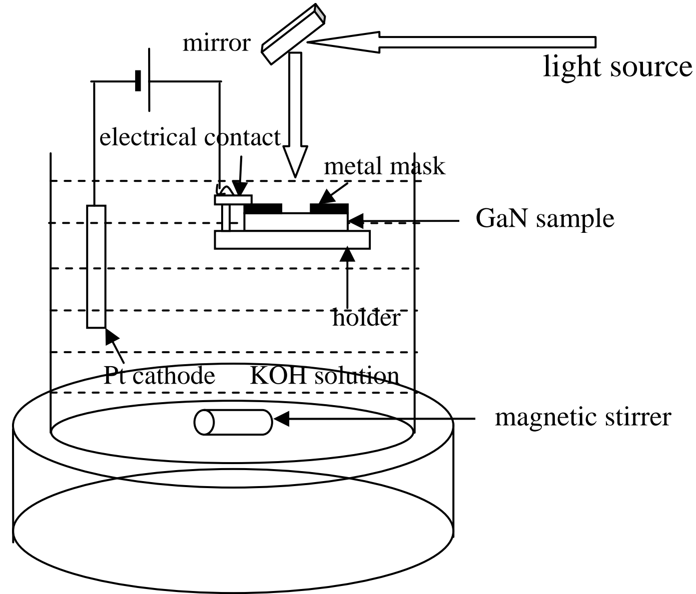

Figure 3.6 Electrochemical cell for electrode PEC wet etching

For ELPEC wet etching, the basic experiment setup was similar to the experimental apparatus, as shown in Figure 3.6. The difference was that there was no Pt cathode used. The strong oxidizing agent $K_2S_2O_8$, mixed together with KOH solution, substituted the Pt cathode in the electrochemical cell. In all of our experiments of ELPEC wet etching, the concentration of $K_2S_2O_8$ was fixed at 0.05mol/l, and the pH value of the solution changed with the various concentrations of KOH being mixed with the $K_2S_2O_8$ solution.

Before etching, the samples were immersed in the 2M KOH solution (pH=14.02) for 10mins as the pre-treatment. It is helpful to remove the native oxide layer on the specimen surface. For systematic study, we varied the light intensity and the concentration of the KOH solution. In addition, we investigated the effects of external power supply, chopper and ultrasonic post treatments after etching. All the

experiments were conducted at room temperature with a 10 rps rotation of the magnetic stirrer.

The following flow diagram shows the experimental processes of PEC wet etching:

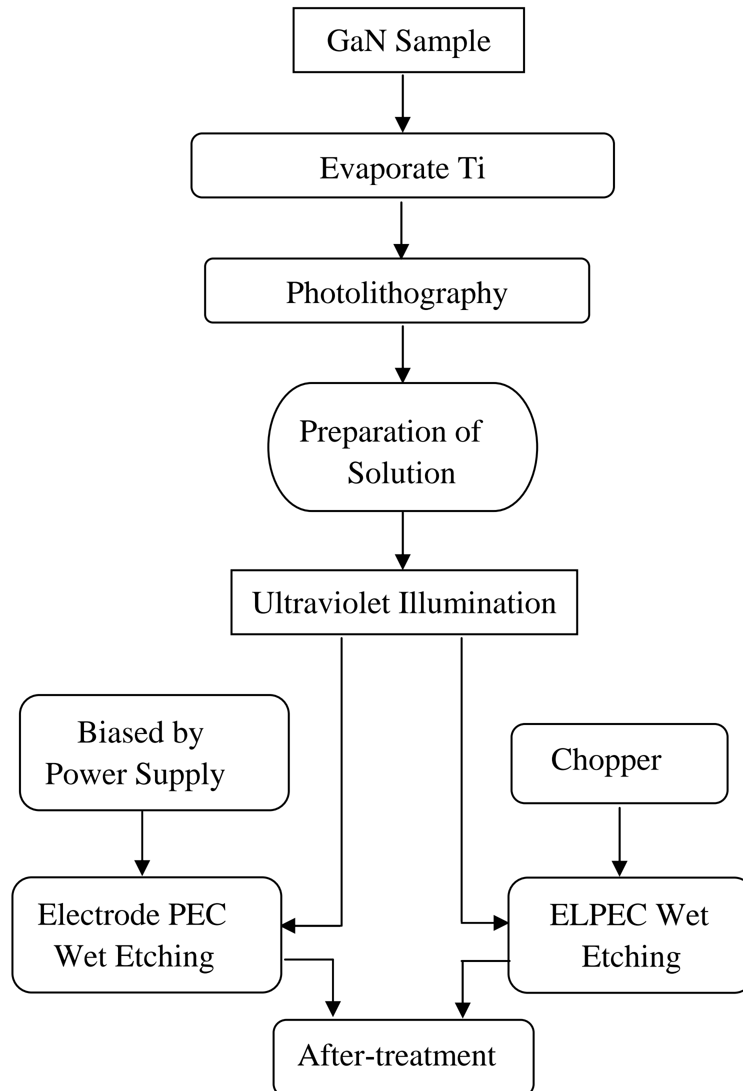

Figure 3.7 Detailed flow diagrams of all the steps in PEC wet etching of samples

3.3 Sample Analyses

The pictures of the corresponding experimental setups for the various experimental characterizations are introduced in this section, as shown below:

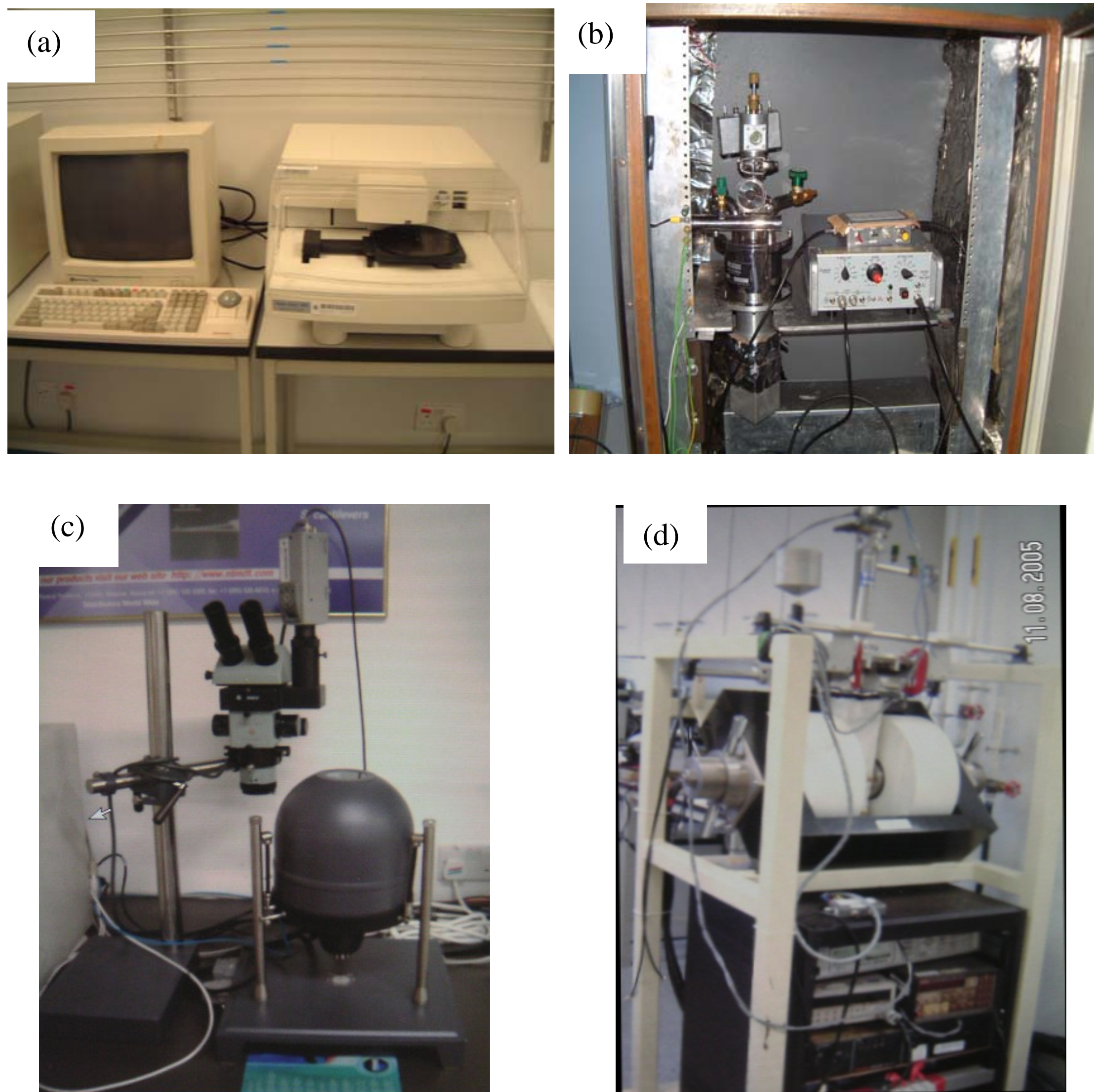

Figure 3.8 (a) α-Step 500 Surface Profiler (b) Shield room for low temperature noise measurement (c) Atomic Force Microscope (d) Hall measurement system

3.3.1 α-Step Experimental Setup

An α-Step 500 Surface Profiler is used to generate profiles of etching depths achieved for each sample, from which the etching rate can be calculated. The specimen was first placed on the holder, and then a stylus is placed in contact with the surface of the sample. The stylus is then made to scan across the sample over a prescribed length. The images were acquired in the length of 500 μm at the speed of 20μm/s. The machine has the ability to fit and level data, allowing accurate measurements on curved surfaces.

3.3.2 Atomic Force Microscope and Scanning Electron Microscope Experimental Setup

The surface morphology was examined by SEM and AFM. The specimens were first cleaned before measurement. To estimate the surface roughness, AFM images were performed in air using the Solver P47 SPM at constant force mode. The largest area for scanning was $10 \times 10\ \mu m^2$. The RMS roughness of the surface roughness was calculated. SEM experiments were performed at Materials Processing Laboratory in the Department of Applied Physics of The Hong Kong Polytechnic University. The samples were first coated with a thin layer of Au metal before measurement by SEM in vacuum. This SEM has a magnification range from 10 × to 100,000 × and the angle of microscope changes from vertical direction to 75 degree bevel. SEM enables one to view the surface morphology in a macroscopic scale and to observe abnormalities like whiskers or pits on the surface of the samples.

3.3.3 Hall Measurement Experimental Setup

Temperature dependent Hall mobility and carrier concentration were measured from the cross-bridge resistive structure in the system shown in Figure 3.8(d). The samples were cooled in an exchange gas liquid nitrogen cryostat with the device temperature varying from 110K to 300K at 10K intervals. The device temperature was controlled by a LTC-11 temperature controller. To conduct Hall-effect measurements as shown in Figure 2.8, the specimens were put in a magnetic field with a magnetic flux density of 0.33T and current bias was applied between contacts 5 and 6 by a Keithley 220 programmable current source. The directions of the magnetic field and the current can be varied. As the Hall voltage V_h is often small of the order several mV, we used the Keithley 2000 multimeter for measurement.

3.3.4 Noise Measurement Setup

Low-frequency noise was investigated as a function of biasing conditions and the device temperature. The device under test (D.U.T) was placed inside a continuous flow cryostat, which can be cooled down to 77K by liquid nitrogen. The temperature was controlled by a Lakeshore 91C temperature controller, which stabilized the device temperature to within 15 mK over the duration of the period for noise data acquisition. During the experiment, the device was biased by a battery-powered current source, which avoids the undesired noise sources from the power supply. The experimental setup to obtain the voltage power spectral density is displayed in Figure 3.9. In order to attain the ac open-circuit condition of a current source, a large

metal-film series resistance R_s was connected to a ten-turn 100k rheostat. The value of R_s should be at least 30 times larger than the ac conductance of the sample [57]. The biasing voltage can be adjusted by the rheostat. To eliminate any extraneous noise from interfering with the results, the cryostat, the biasing circuit and PAR113 low-noise preamplifier to amplify the fluctuating voltage across the device were enclosed in a shielded room, as shown in Figure 3.9. The amplifier has a maximum gain of 1000 and a maximum upper roll-off frequency of 1 MHz. The amplified noise was coupled to an HP3516A dynamic signal analyzer for data collection. For accuracy, the noise spectra were averaged 1000 times. To investigate the low-frequency noise of the sample from cross-bridge structure (shown in Figure 2.8), first a constant current bias applied between contacts 5 and 6. The voltage noise power spectral density was then measured across contacts 2 and 3 or 1 and 4. In this way, the contact noise does not contribute to the total noise of the structure [71].

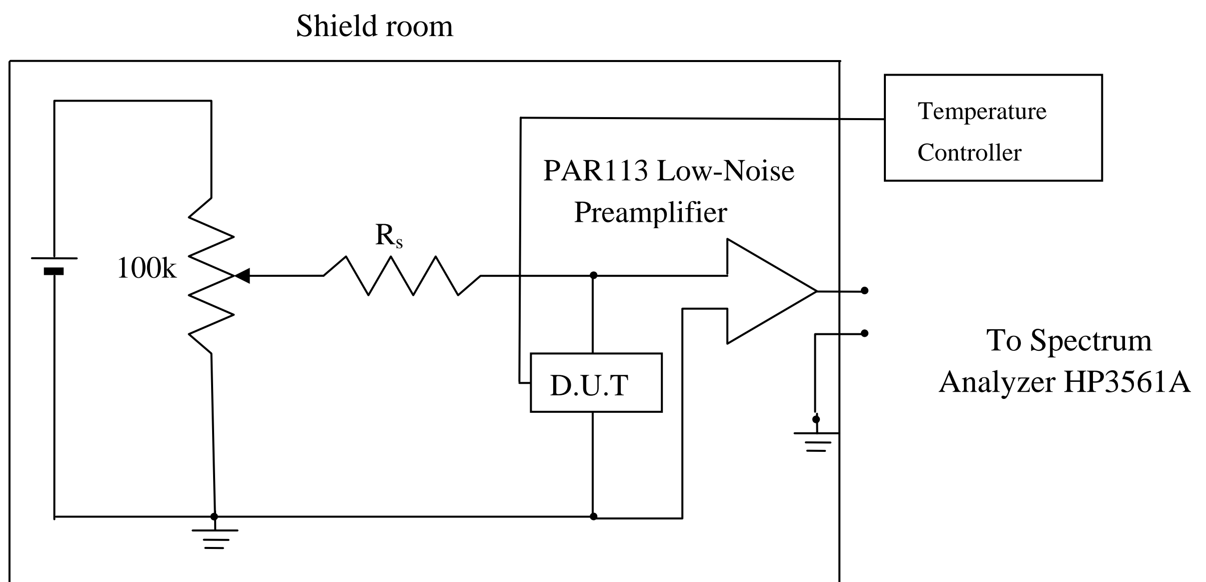

Figure 3.9 The experimental setup for noise measurement

Chapter 4. Experimental Results

This chapter is divided into two parts: one part is about the experimental results on the characterizations of the etching rates and surface morphology of the etched samples; the second part is on the electrical properties and low-frequency noise of cross-bridge structures fabricated using different etching conditions. Experimental results are concisely commented as necessary, while detailed discussions will be presented in the next chapter.

4.1 Results of PEC Wet Etching and Corresponding Characteristics

4.1.1 Electrode PEC Wet Etching for n-type GaN

N-type GaN samples were patterned with circular holes on Ti mask as indicated in Figure 3.1. A 300W xenon lamp was used as the light source. The influences of light intensity, concentration of the solution, and external biasing on the etched GaN films were all investigated. First, the experiments were conducted at a constant light intensity of 20mW/cm^2 for half an hour in different concentrations of the solution without any bias, i.e. 0.01M KOH (pH=11.98), 0.1M KOH (pH=12.76) and 0.5M KOH (pH=13.50). To investigate the effect of light intensity on the etching rate the specimens were placed in a 0.1M KOH solution and were irradiated with light intensity varying between 10mW/cm^2 and 30mW/cm^2. The experimental results are shown in Figure 4.1 and Figure 4.2. The maximum etching rate reaches about 16nm/min in 0.1M KOH at 30mW/cm^2 light intensity without the application of a bias.

It is observed that the etching rate increases with light intensity and concentration of the solution. Moreover, the correlation between etching rate and solution concentration shows saturation trend when the samples are etched in higher concentrations of the solution. The onset of saturation represents a transition in the reaction limitation. At saturation, the reaction rate shifts from being limited by the dissolution of the surface oxide to being limited by the rate of the oxidation reaction itself.

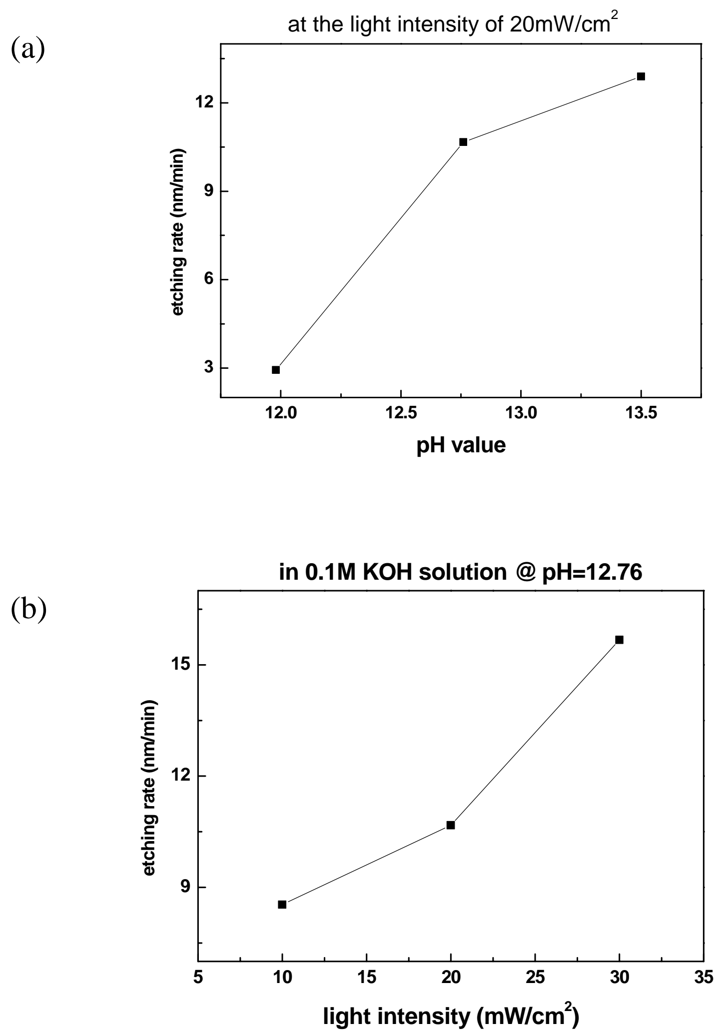

Figure 4.1 Dependences of etching rate on (a) concentration of the solution and (b) light intensity without any bias.

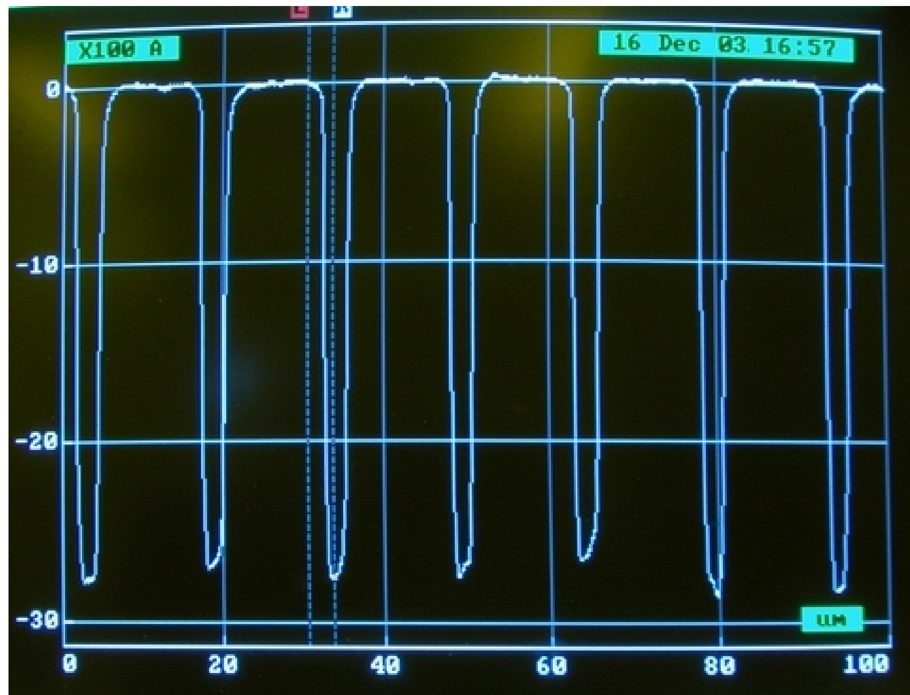

Figure 4.2 α-Step profile of a typical PEC wet etching with holes as pattern

In addition, the surface morphology as a function of solution concentration was investigated using SEM. Figures 4.3(a)-(c) show the trends of surface morphology with the increasing solution concentration, using 0.01M KOH, 0.1M KOH, and 0.5M KOH in sequence. The variation in the surface morphology exhibits an even more complex behaviour. The different etching regimes allow the etching process to be tailored to the characterization of crystalline quality and defect density of the etched sample, as well as the various etching selectivity arising from different surface reaction kinetics. The detailed comments will be made in the next chapter. The experimental results on the etching of n-type GaN by electrode PEC wet etching technique, as mentioned above, are well consistent with the previous reports [12,70].

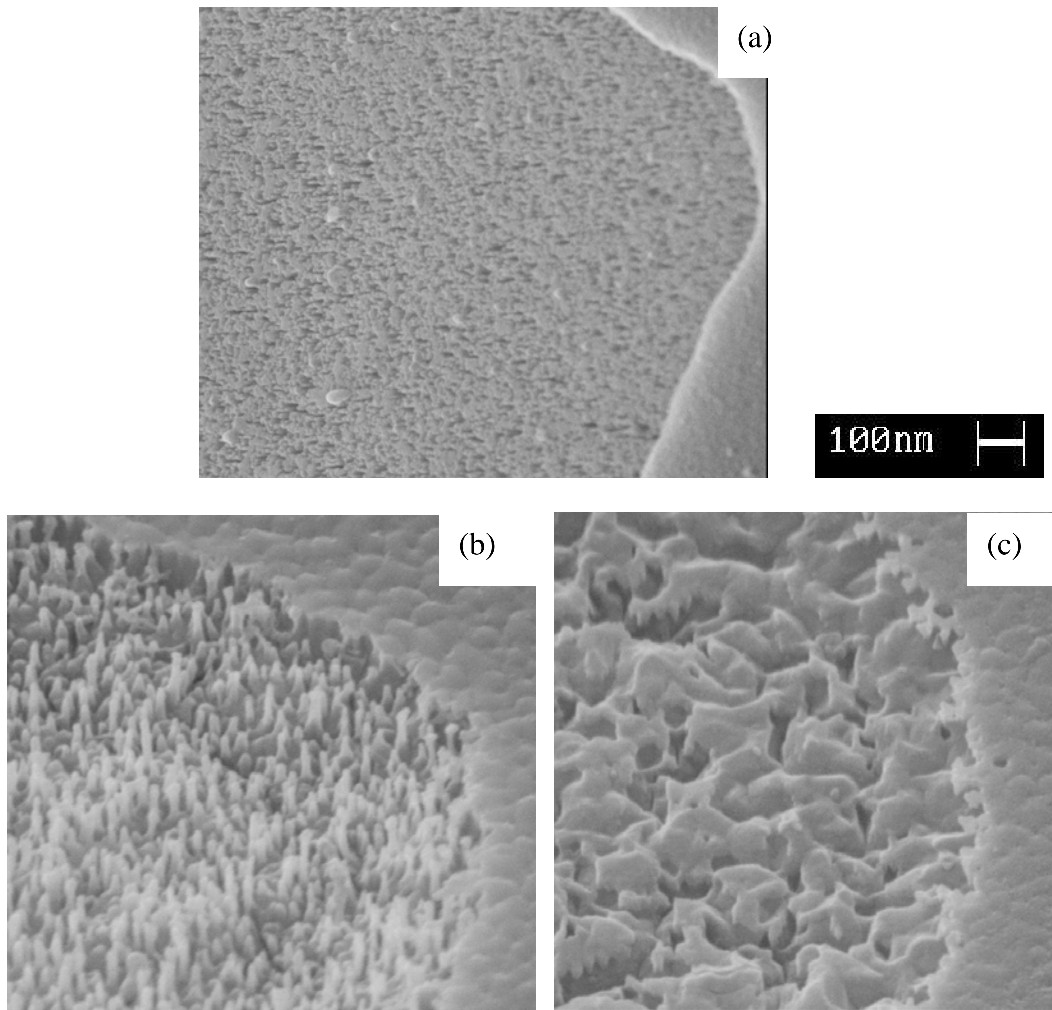

Figure 4.3 Collage of different categories of surface morphology: (a) intermediate smooth etch and dislocation decoration (b) columnar nanostructure (c) nanometer etch pits

Moreover, the different etching rates by the reason of the sample geometry were observed in the experiments. Using a Hall Bar structure (as shown in Figure 3.2) with the distance of 500 μm between every two devices, the GaN material was etched away forming a mesa structure. The experiment was repeated using solutions with different concentrations. It is found that when the concentration of solution is low, such as 0.01M KOH and 0.1M KOH, the etching rate is larger around the edge of the masked

region than that at the centre of the etched region, as shown in Figure 4.4. Such a phenomenon is not observed when the 0.5M KOH solution was used. This can be explained by local variations in the concentration of the solution. The situation is particularly serious under conditions where the concentration of the reagent is low. In this case it is expected that the process is dominated by the mass transport of reagents to the etching surface.

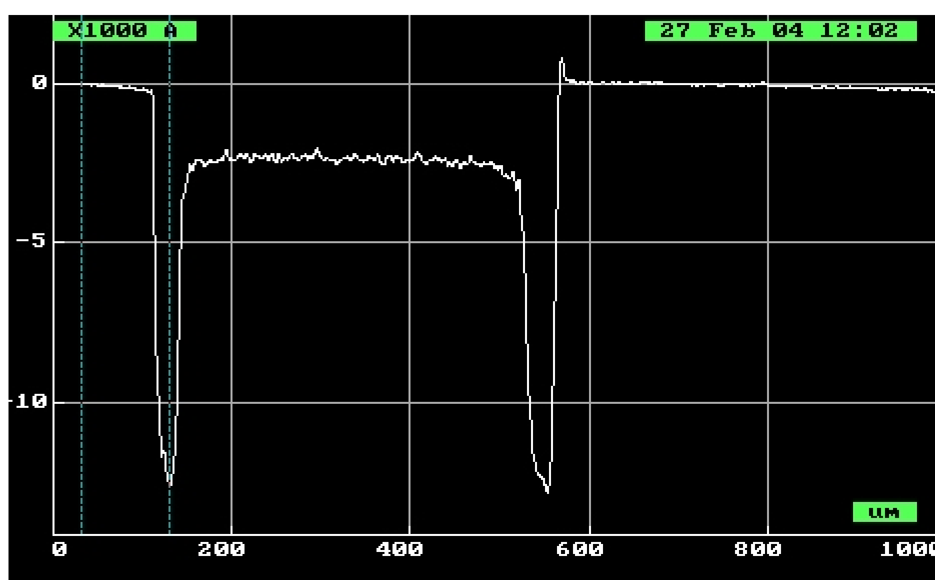

Figure 4.4 α-Step profile of large area etching in 0.01M KOH

The basic principle of PEC wet etching is the redox reaction in which both electrons and holes must exist. Since a constant current source can supply both electrons and holes to the anode and the cathode respectively via an external circuit in electrochemical cell, etching rate will increase with a rise in the applied current density. N-type GaN films were illuminated under a UV light intensity of $30mW/cm^2$ in a 0.1M KOH solution. The etched area of the sample was $3\times3mm^2$ using the

following currents: 0.21mA, 0.5mA, 1mA, and 3mA. Figure 4.5 shows that the etching rate increases with the applied current density. The maximum etching rate is 83nm/min with 33mA/cm^2 current density applied. In addition, it also shows a saturation in the etching rate in the high current density range, which means the redox reactions reach saturation with redundant electrons and holes. In this situation, concentration of the solution and the conductivity of the GaN film would be the limiting factors for etching rate.

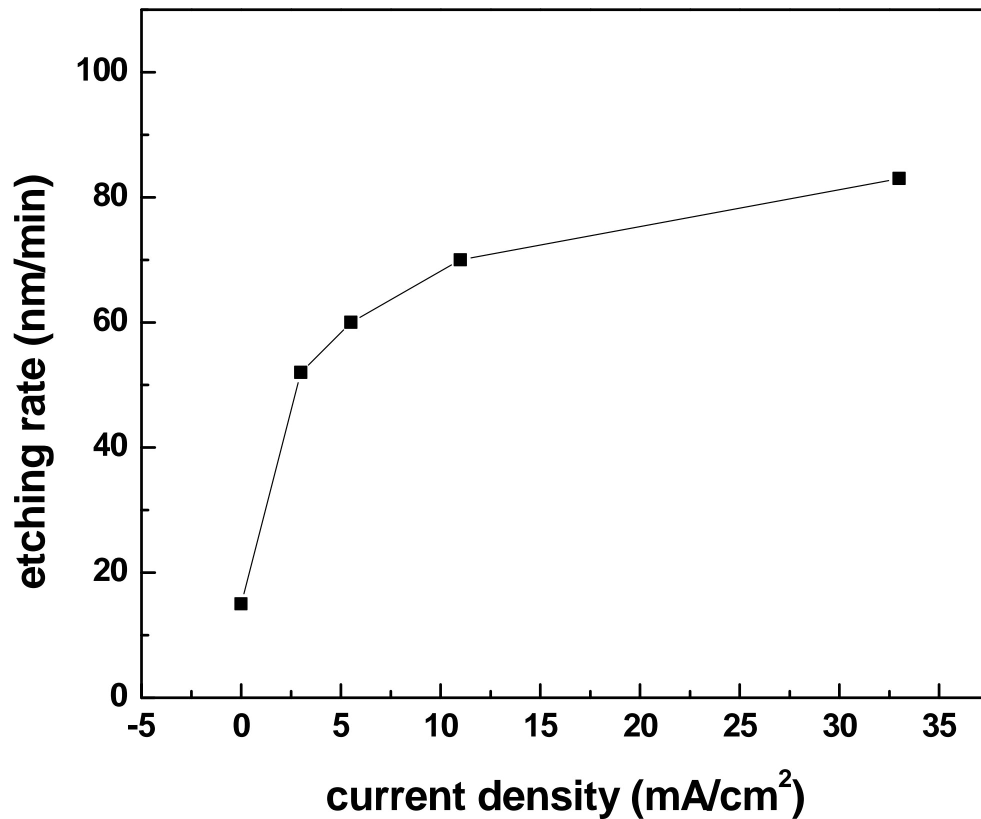

Figure 4.5 Etching rates variation with current density

4.1.2 Electrode PEC Wet Etching for Undoped GaN

Although the theory and other related reports indicate that electrode PEC wet etching for undoped GaN is difficult to realize [19,20,24], the wide applications of high-quality undoped AlGaN/GaN heterostructures in electrical and optical devices and the great benefit of wet etching in device performance have made the relevant research more important. This section focuses on the technique for undoped GaN using electrode PEC wet etching.

Mesa etching is needed to isolate the devices from each other. One important purpose is to eliminate leakage current among them. It needs to achieve a complete and thorough etching over a large area. Based on the experimental results on n-type GaN etching, the undoped GaN sample with cross-bridge pattern was placed in a 0.5M KOH solution under 30mW/cm^2 illumination intensity. After an hour of etching without biasing, we found that only the region around Ti mask was etched and the etching rate was as slow as 10Å /min. In order to increase the etching rate, we applied a positive bias in the external circuit, heated the solution to 60℃ and used a chopper to modulate the incident beam [27,28]. However, these techniques do not work well. Typical etched pattern is shown in Figure 4.6, which indicates that there exists an uneven etching over a large area. The region close to the device is etched much more deeply. Figure 4.7, which shows the time dependence of the photocurrent during the etching process, gives a hint for the reason why etching is so difficult for undoped GaN. Figure 4.7 indicates that the photocurrent falls to 1μA within 5 minutes for

undoped GaN, while for n-type GaN the photocurrent remains at over 10μA throughout the period. Since photocurrent is an indication of the etching rate, it is obvious that etching nearly stopped after 5 minutes for undoped GaN films. There are two main reasons for this observed phenomenon. Firstly, for undoped materials the Fermi level is located close to the middle of the bandgap, as a result there are very few electrons and holes available at the GaN/KOH interface where the redox reaction takes place; secondly, the high resistance of undoped GaN substantially lowers the rates of electrons and holes being transported to the interface. Both these factors result in the low rate of the redox reaction.

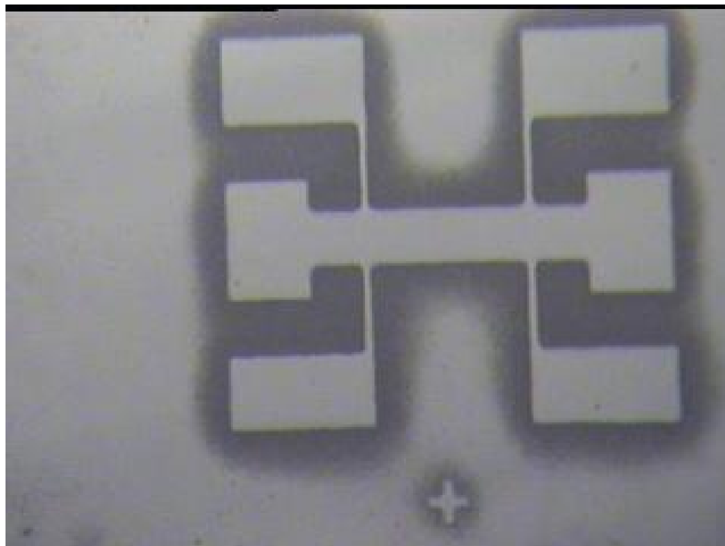

Figure 4.6 Undoped GaN sample after PEC wet etching: the dark part was etched.

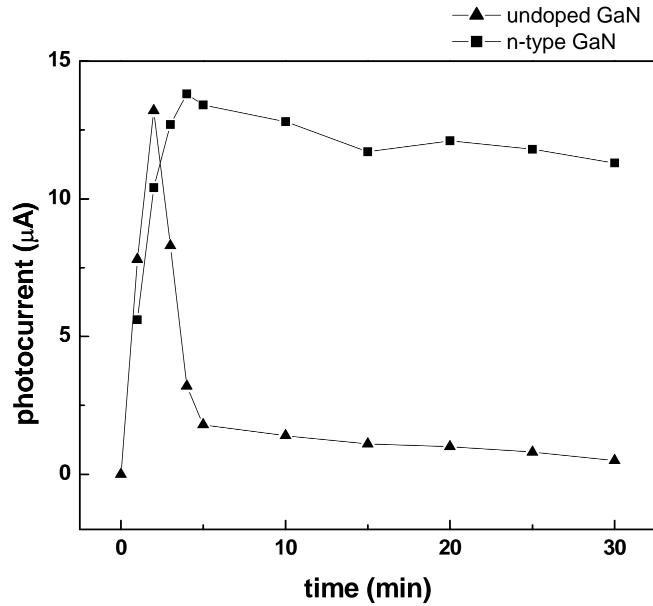

Figure 4.7 Photocurrents for n-type and undoped GaN at the same condition

4.1.3 Electrodeless PEC Wet Etching for Undoped GaN

According to the above results, electrode PEC etching technique is not suitable for etching undoped GaN materials. We have considered applying an alternative approach – electrodeless PEC wet etching, for the etching of undoped GaN. Based on the mechanism of ELPEC wet etching, $K_2S_2O_8$ reacts with an electron to generate a hole at the GaN/electrolyte interface. This process increases the hole concentration at the GaN/electrolyte interface. At present, ELPEC technique is typically applied for the etching of undoped GaN, as a substitute for electrode PEC wet etching. Using the mixture of 0.1M KOH and 0.05M $K_2S_2O_8$ as electrolyte, the best result was obtained under 30 mW/cm^2 light intensity without chopper. The maximum etching rate was about 25Å/min. But this etching rate is still too slow for mesa etching. Compared with the conditions reported by other groups, we selected a higher intensity light source –

the HeCd laser which emits a coherent light at 325 nm, to replace the 300W xenon lamp so as to improve the etching rate.

ELPEC etching was performed in the experimental setup described in chapter 3.2.2. To obtain an optimal etching condition for the undoped GaN samples, we first systematically examined the effects of the light intensity and the concentration of the solution on the etching rate and the surface morphology. The maximum intensity that can be achieved by the HeCd laser is 1.68W/cm^2 at 325nm and the minimum intensity is 0.64 W/cm^2 accomplished by using an attenuator. The pH values of the electrolytes ranged from 12 to 14 with the variation of the concentration of KOH solution from 0.01M to 0.5M. The results are shown in Figure 4.8 and Figure 4.9. It can be observed that a peak etching rate of 22 nm/min is achieved with a pH value of 12.8 (0.1M KOH+0.05M $K_2S_2O_8$) under the maximum light intensity, and the surface roughness of the film is found to increase with the increment of concentration. On the other hand, it is observed as the light intensity increases, the etching rate increases monotonically and the RMS roughness, examined by AFM, is found to be the lowest. If fitting the curves in Figure 4.9, it seems to show a linear relationship with the variation of light intensity. From Figure 4.8, the smoothest surface is obtained in the solution of 0.01M KOH and 0.05M $K_2S_2O_8$. The RMS surface roughness is 10.53nm, which is comparable to 11.47nm for the as-grown sample. A typical AFM image of the etched surface is shown in Figure 4.10.

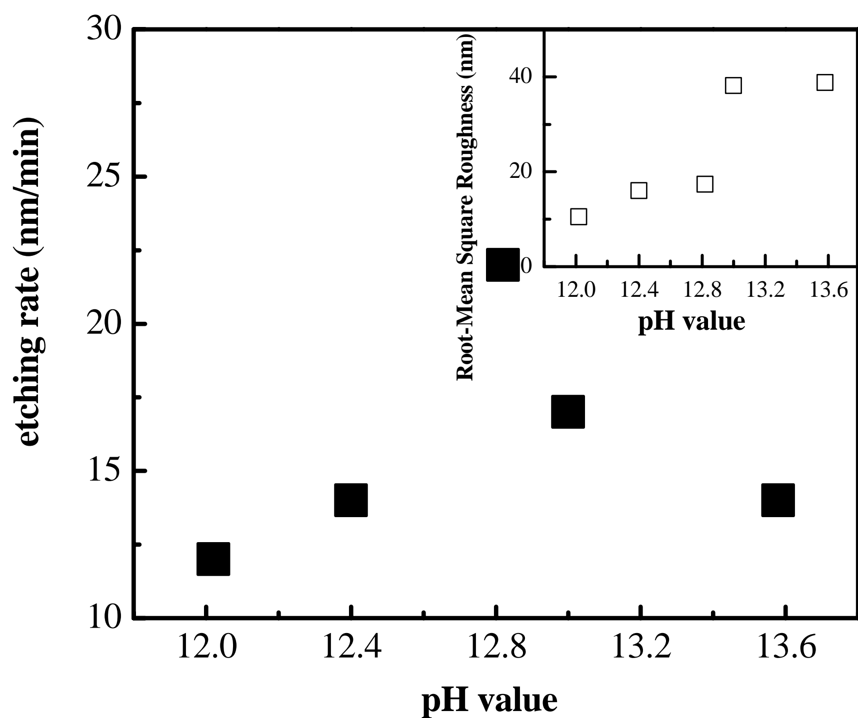

Figure 4.8 Etching rates and RMS roughness of the etched surface varied as a function of the pH value at the light intensity of 1.68 W/cm^2.

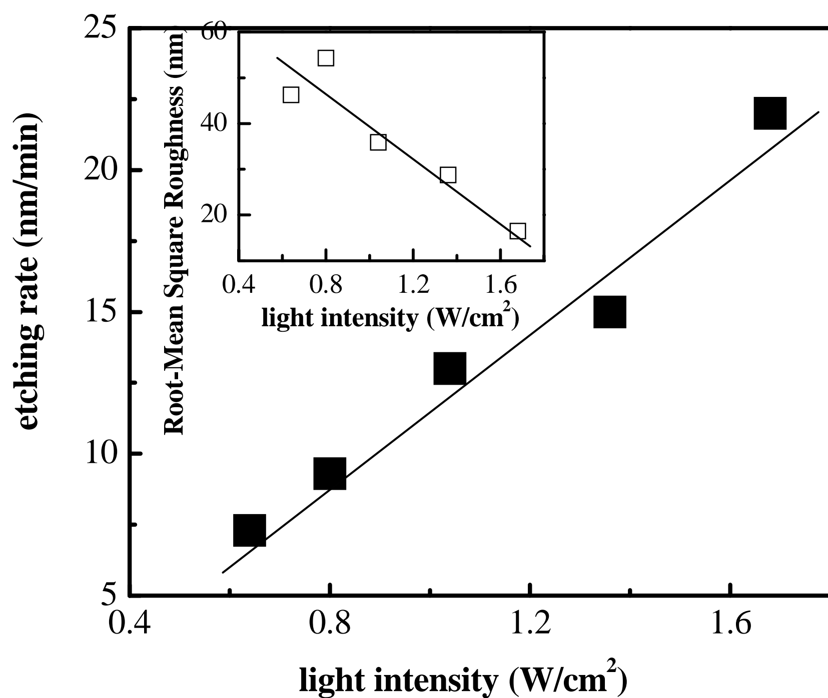

Figure 4.9 Etching rates and RMS roughness of etched surface as a function of the light intensity in a 0.1M KOH and 0.05M $K_2S_2O_8$ mixture.

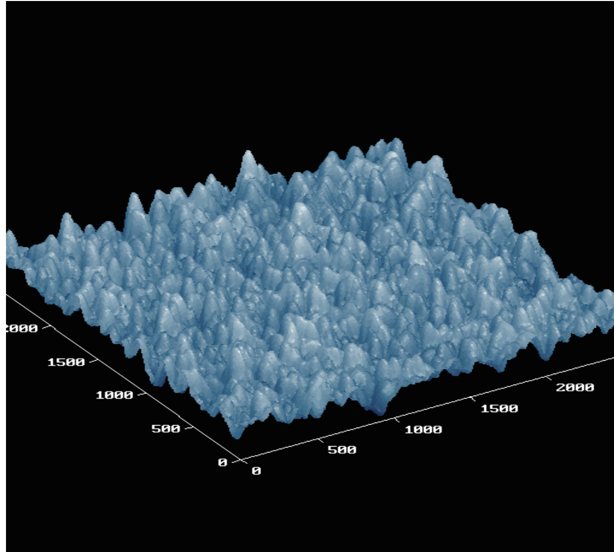

Figure 4.10 AFM image of the etched undoped GaN sample

As shown in Figure 4.8, although the RMS roughness for the etched surface in the 0.01M KOH solution is a little smoother than the rest, the etching rate is about two times slower than that obtained in the 0.1M KOH solution. Hence, as a trade-off between the etching rate and the surface morphology the optimal concentration is taken to be a mixture of 0.1M KOH and 0.05M $K_2S_2O_8$ which as a pH value of 12.67 as shown above. The samples were etched in a mixture of 0.1M KOH and 0.05M $K_2S_2O_8$ at the light intensity of 1.68W/cm^2 were further investigated. It was found that the etched surface become much smoother after ultrasonic treatment with in a 2M KOH solution at 60ºC, as indicated by the SEM pictures in Figure 4.11. Using AFM characterization we found that the RMS roughness decreased from 17.379nm to 8.482nm after the ultrasonic treatment. In addition, J. M. Hwang *et al.* [28,72] reported that the ELPEC etching with a chopped UV source could get smooth etched surface. However, when we used a chopper at the frequency of 2.5 kHz during the

etching process, the etched surface became very rough, as shown in Figure 4.12. The RMS roughness is as large as 60.761nm, which indicates that the effect of chopped PEC etching on GaN is much diverse for different samples. More detailed investigation of the mechanism of ELPEC etching with the use of a chopper is needed to understand the phenomenon.

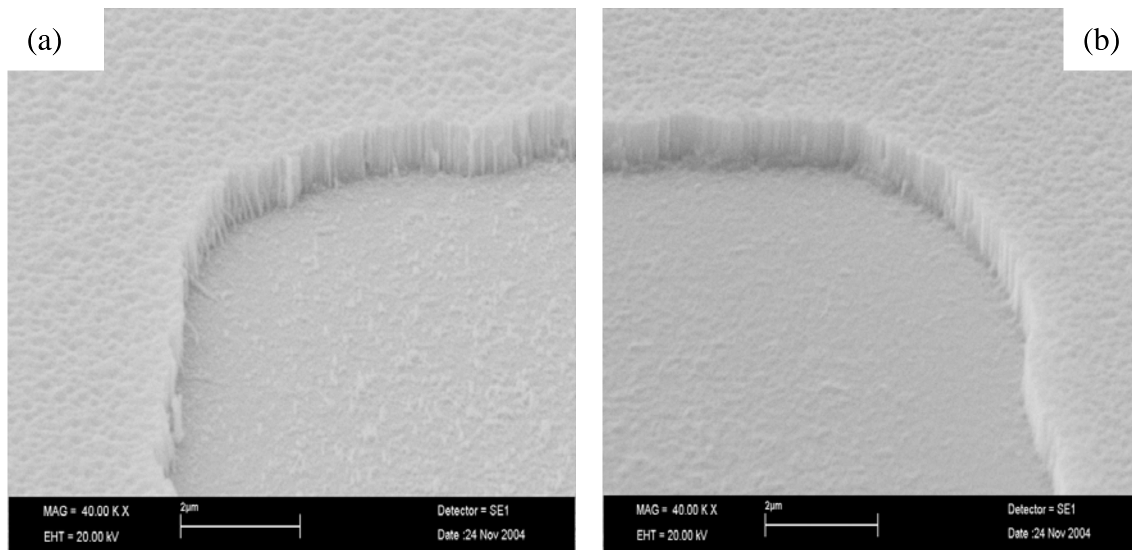

Figure 4.11 (a) undoped GaN film etched in 0.1MKOH+0.05M$K_2S_2O_8$ solution; (b) After ultrasonic treatment in 2M KOH solution at 60℃ for 10 minutes.

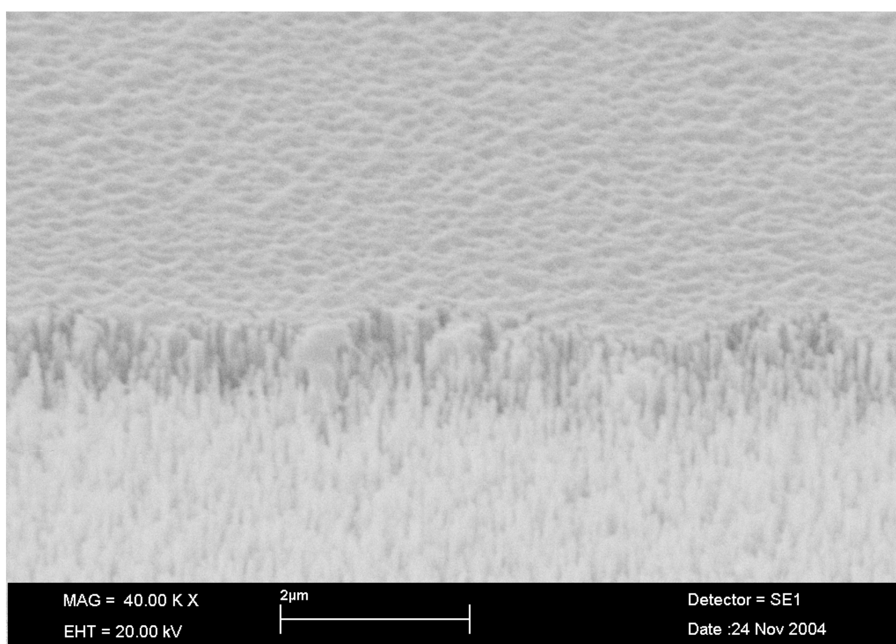

Figure 4.12 SEM micrograph of undoped GaN sample etched with chopped light source

4.2 Characteristic Analyses of Cross-bridge Structures Fabricated on AlGaN/GaN Heterostructures

Due to the existence of a two-dimensional electron gas (2-DEG) channel which demonstrates high mobility, low resistance and low noise performance, electronic devices fabricated on AlGaN/GaN heterostructures have found important applications in power microwave devices. One of the focuses of our project is to investigate the fabrication and characterization of the cross-bridge structure using AlGaN/GaN heterojunctions by PEC etching technique. The process may have an important potential in device applications. In this section, characterizations on the influences of the etching process on device performance are examined on cross-bridge structures for undoped AlGaN/GaN heterostructure films.

4.2.1 Mesa Isolation Obtained by Electrodeless PEC Wet Etching

The AlGaN/GaN heterostructure consists of an undoped AlGaN film that was deposited on an undoped GaN layer. In our studies, we have performed ELPEC wet etching for undoped GaN layer. It has been pointed out that the etching rate of AlGaN is higher than that of GaN [13]. A typical graph on the temperature dependence of Hall mobility and sheet carrier concentration of AlGaN/GaN heterostructure is shown in Figure 4.13. It is found that Hall mobility shows a monotonic increase with the decreasing temperature, which indicates typical 2-DEG temperature dependence of the carrier mobility [74,75]. At room temperature, the Hall mobility is 760 cm^2/Vs and increases to 1100 cm^2/Vs at 130K. Meanwhile, sheet carrier concentration of

2-DEG also increases from 5.5×10^{12} cm^{-2} to 6.5×10^{12} cm^{-2} as the temperature decreases from 300K to 130K.

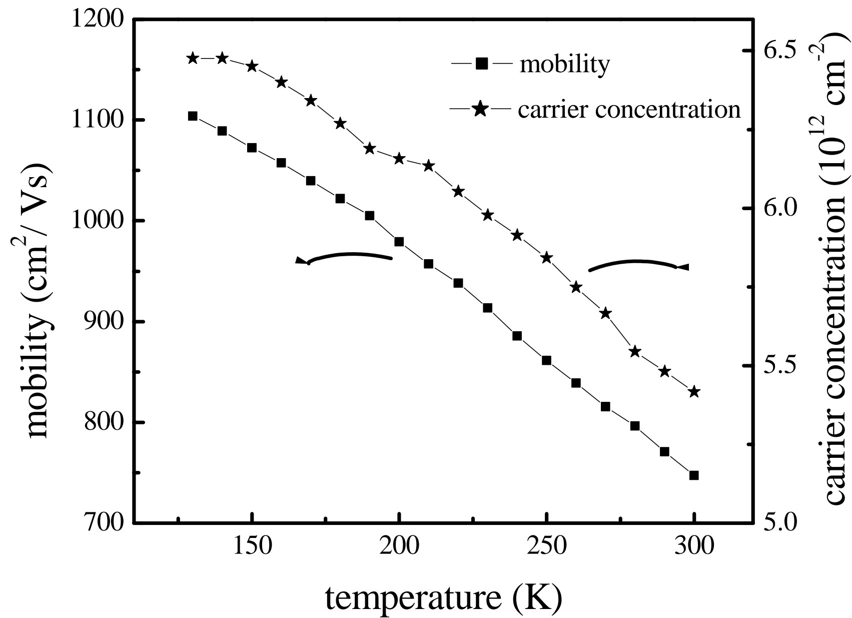

Figure 4.13 Hall electron mobility and sheet carrier concentration of the AlGaN/GaN heterostructure versus temperature

In order to carry out a systematic study, cross-bridge mesas on AlGaN/GaN heterojunctions were etched under different etching conditions. The dimension of the cross-bridge structures was 110μm×10μm. All samples underwent ultrasonic treatment after etching for 10 minutes at 60℃. Five different concentrations of the solution were used at the light intensity of 1.68 W/cm^2 and the devices were named according to Table 4.1. Also, the devices fabricated using different light intensities in the mixture of 0.1M KOH and 0.05M $K_2S_2O_8$ are labelled according to Table 4.2. These two tables are shown as below:

Table 4.1: Devices etched at a constant light intensity of 1.68 W/cm^2

Concentration of the solution	**Device**
0.01M KOH + 0.05M $K_2S_2O_8$	A
0.05M KOH + 0.05M $K_2S_2O_8$	B
0.1M KOH + 0.05M $K_2S_2O_8$	C
0.2M KOH + 0.05M $K_2S_2O_8$	D
0.5M KOH + 0.05M $K_2S_2O_8$	E

Table 4.2: Devices etched at a constant solution concentration of 0.1M KOH and 0.05M $K_2S_2O_8$

Light intensity	**Device**
1.36 W/cm^2	F
1.04 W/cm^2	G
0.80 W/cm^2	H
0.64 W/cm^2	J

Under each etching condition, several devices were measured. The Hall mobility was measured at room temperature. Figure 4.14 indicates the corresponding mobility as a function of the concentration of the solution and the light intensity. Our devices are fabricated within the same general region of the wafer. However, there exist some differences among the devices from the same wafer. The typical variation of the mobility within the same wafer is about 5%. Also low-frequency noise measurement is measured to evaluate the performance of each device. Low-frequency noise is a particularly important parameter for the characterization of the film quality because it has been shown that the noise power spectral density is directly proportional to the

defect density in the film. The experimental results in Figures 4.15 and 4.16 are the typical experimental data, which are all taken with the devices being current bias at 0.2V by an all-passive current source with the output resistance of 10MΩ. As can be seen from these figures, the voltage noise power spectral density, $S_V(f)$, varies systematically from device to device. The data show that the conditions of ELPEC wet etching not only affect the etching rate and surface morphology, but also have strong effects on electrical properties and low-frequency noise of films.

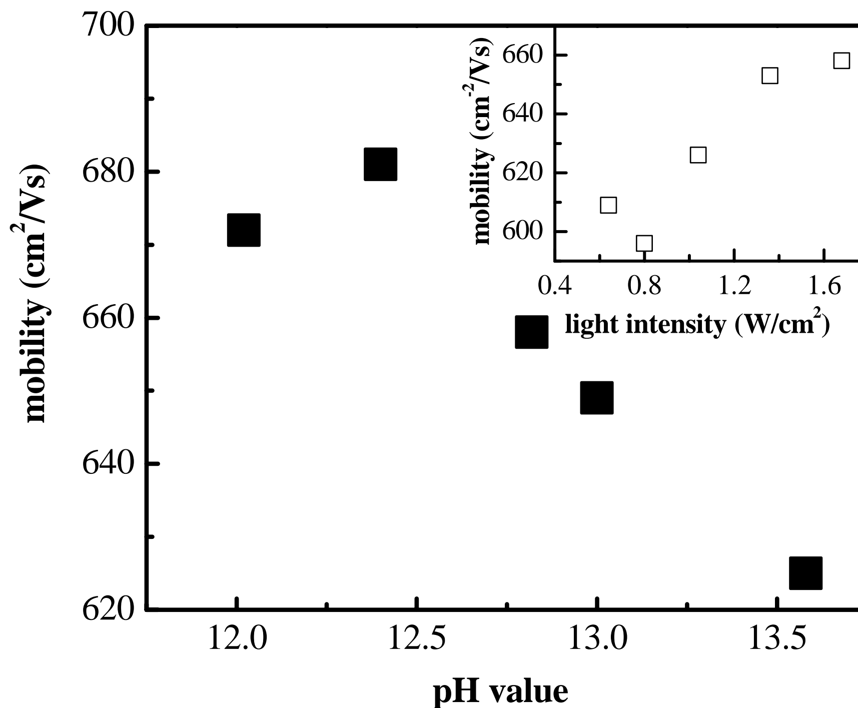

Figure 4.14 Room temperature Hall mobilities as a function of concentration of the etching solution and light intensity.

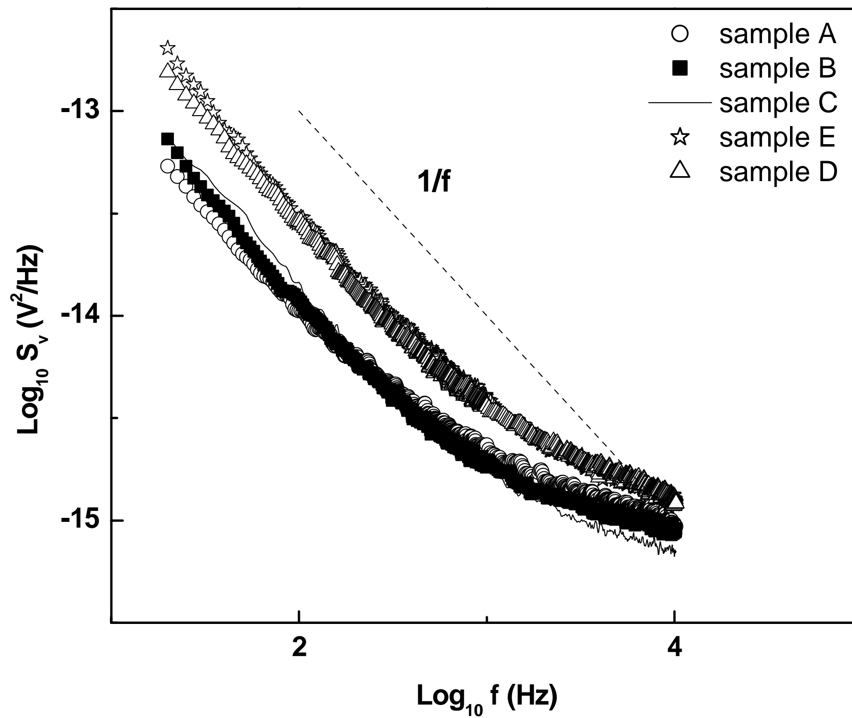

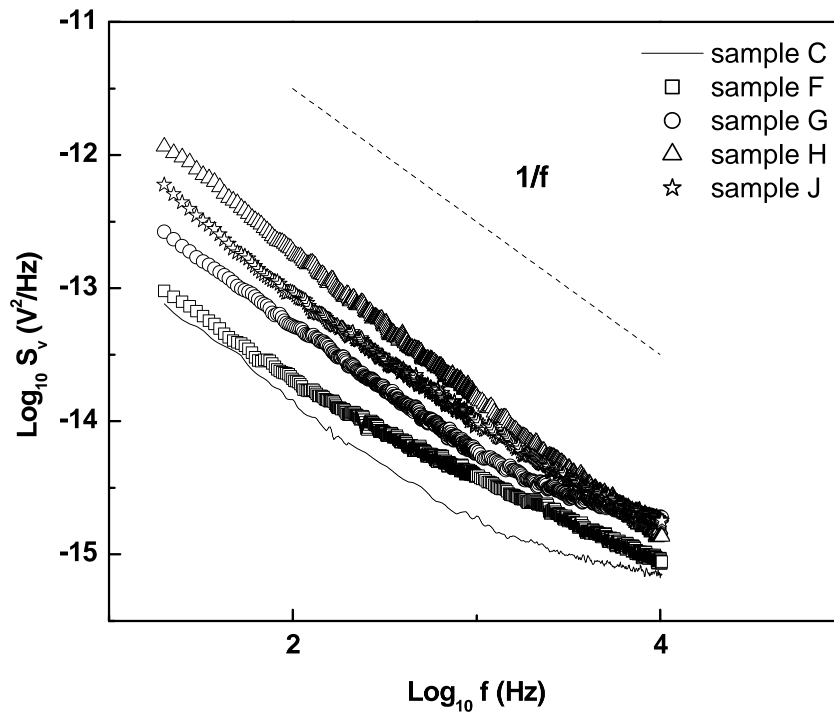

Figure 4.15 Room temperature voltage noise power densities of cross-bridge structures fabricated with different concentrations of the solution and light intensities

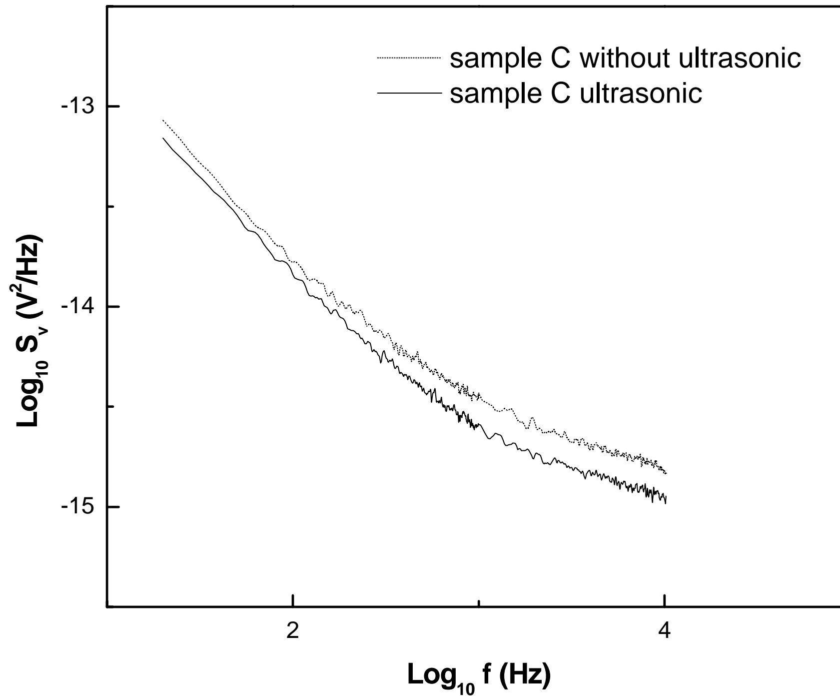

Figure 4.16 Experimental $S_V(f)$ measured before (dashed line) and after (solid line) ultrasonic treatment in 2M KOH solution at 60°C

In particular, we selected devices C, E and H for low temperature noise measurements from 90K to 300K. Temperature dependencies of $S_V(f)$ at the frequency of 120Hz are sketched in Figure 4.17 for comparison. The three curves appear to have a similar trend as the temperature varies. Although the experimental results show that at low temperature, $S_V(f)$ is dominated by flicker noise for samples C, E, and H, two G-R pumps are seen to superimpose with the flicker noise power spectra as shown in Figure 4.17, at about 100K and 300K respectively. A Lorentzian bump was observed at low temperature in sample C, which was fabricated in the mixture of 0.1M KOH and 0.05M $K_2S_2O_8$ under a light intensity of 1.68 W/cm^2. The presence of a G-R bump can be seen more clearly in a Log_{10} [$S_V(f) \times f$] plot as

shown in Figure 4.18. The figure shows that the cut-off frequency of the Lorentzian, f_0, systematically shifts toward higher frequency as the temperature increases.

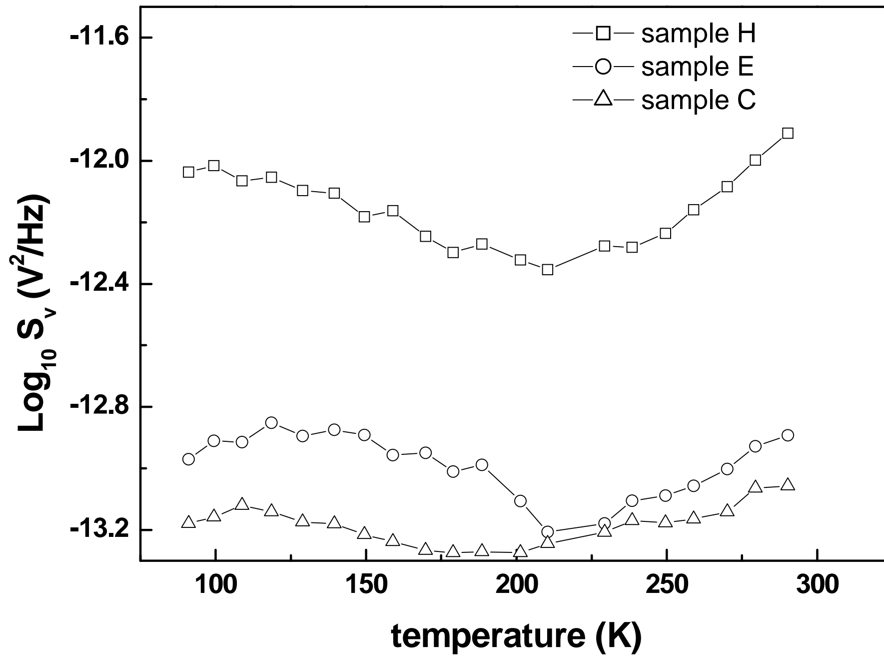

Figure 4.17 Temperature dependence of S_V (f =120Hz) for devices H, E and C

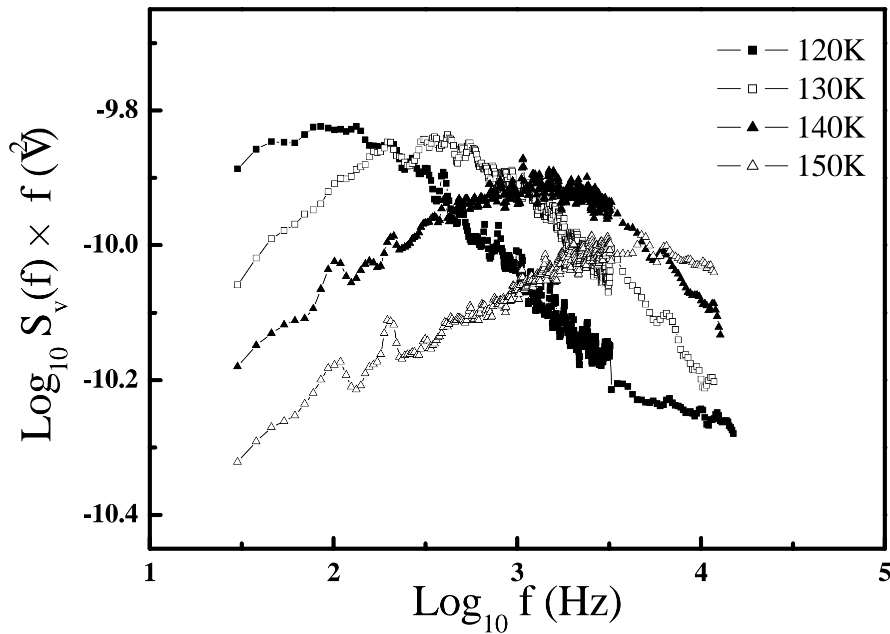

Figure 4.18 Typical experimental results on $S_V(f) \times f$ for sample C from 120K to150K

4.2.2 Mesa Isolation Obtained by ICP Wet Etching

The main intention for our work on PEC wet etching is to replace the traditional dry etching technique for device fabrication. The supreme merit for PEC wet etching is that this process has the potential for inducing less material damage at the etched surface and the sidewall of the device. Hwang *et al*. [81] reported that PEC wet etching with a post-treatment method provided a near damage-free etching. To validate that PEC wet etching is indeed a better way to fabricate GaN devices with high quality and good performances, we conducted the experiments as below. We fabricated two types of cross-bridge devices on the same wafer. The growth and fabrication processes for both devices are identical, except the different etching techniques to obtain mesa structure. One device named by sample K was etched by inductively coupled plasma (ICP) dry etching technique conducted at The Hong Kong University of Science and Technology. Electron mobility and low-frequency excess noise as a function of the device temperature were measured systematically from the device. The results are compared to that obtained from device C. The experimental data are shown in Figures 4.19 and 4.20. The insert of Figure 4.20 clearly presents typical quadratic dependence of $S_V(f)$ on the voltage bias of the device. This shows that the noise originates from the device itself rather than arising from other extraneous noise. And the results on electronic properties of devices fabricated by ELPEC etching are better. Hooge parameter calculated from Eq. (2.2.12) for device C is found to be ~ 2×10^{-3} at room temperature, while the device K that is fabricated by ICP dry etching, has a Hooge parameter of ~ 9×10^{-3}. However, compared Figure 4.19

with Figure 4.14, the Hall mobility of those devices fabricated by ELPEC technique has a great difference. In order to confirm that it is caused by the non-uniformity of sample itself, rather than the uncertainty of the experimental processes, we fabricated some other devices in the adjacent region of the same wafer using the same processes as described above. The Hall mobilities of these devices at room temperature are also found to be approximately 750 cm^2/Vs.

For the sake of establishing the validity of the results above, five devices of each kind were measured. The standard deviation of these data can be calculated from:

$$< S_V > = \frac{1}{5}\sum_{n=1}^{5} S_{Vn} \qquad \text{and} \qquad \overline{S_V} = \frac{1}{5}\sum_{n=1}^{5}(S_{Vn} - < S_V >)^2 \quad , \tag{4.2.1}$$

where S_V is evaluated at 120Hz, obtained at room temperature with the devices under current bias at 0.3V. The calculated values of $\overline{S}_{ICP}$ and $\overline{S}_{PEC}$ are found to be within the same order of magnitude.

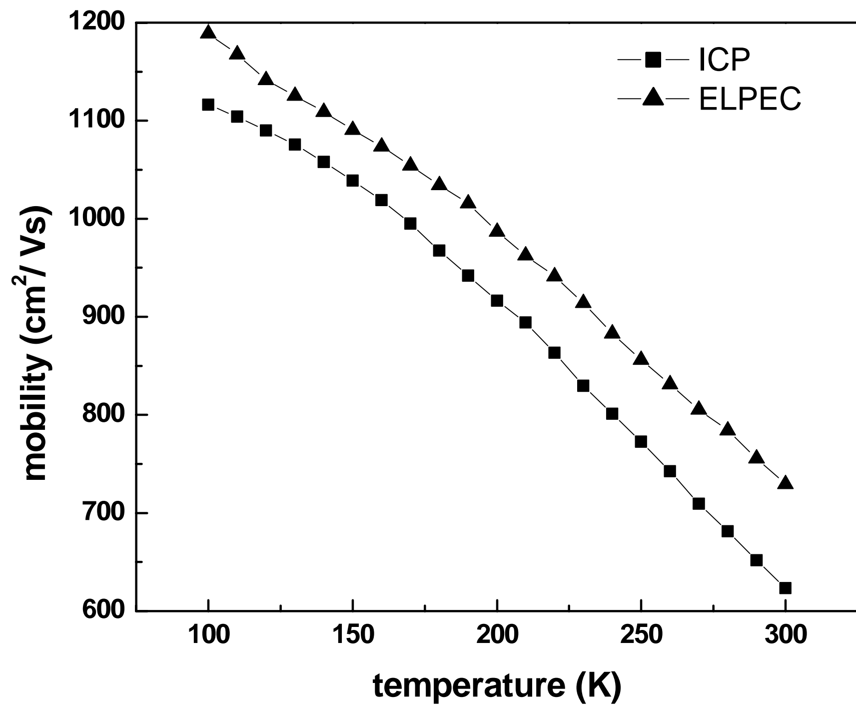

Figure 4.19 Hall Mobility varies with temperature for ELPEC and ICP devices

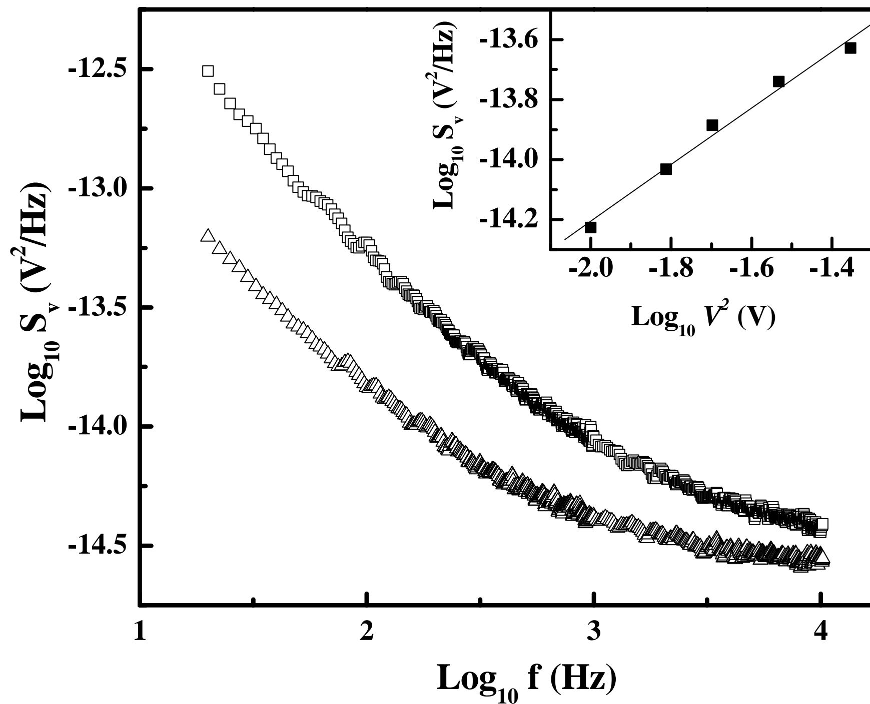

Figure 4.20 Room temperature $S_V(f)$ of ELPEC- (triangle) and ICP- (square) etched devices

Chapter 5. Discussions

Our experimental results show that the morphologies of the samples are strongly influenced by a large number of parameters and experimental conditions. Therefore, optimizing the conditions for a specific GaN sample to achieve smooth, device-quality etched surface is challenging for PEC wet etching. Besides the different conditions for PEC wet etching, the nature and degree of material doping, the uniformity of the doping, and the quality of the original material itself may well determine the etching rates and surface morphology.

First, the relationships between parameters and etching characteristics, like etching rates and the roughness of etched surface, are discussed based on the above experimental results. Both the electrode PEC and ELPEC wet etching exhibit strong dependencies on the light intensity and the concentration of the etching solution, as shown in Figures 4.1, 4.8, and 4.9. As previously stated in Eq. (2.2.1) and Eq. (2.2.2), the dissolution of GaN in electrolyte is a two-step reaction process, involving the formation and dissolution of surface oxides. The number of holes generated by UV light at the GaN/electrolyte interface and the concentration of the electrolyte play important roles in the PEC wet etching of GaN. As light intensity increases, etching rates increases correspondingly until a saturation phenomenon at high light intensity in theory, at which the speed of dissolution of the surface oxides becomes the limiting factor. Similarly, as the concentration of solution increases, the etching rate increases accordingly until a saturation point is reached, at which the speed of the formation of

the surface oxides is the limiting factor in the etching process. However, as shown in Figures 4.1(b) and 4.9, the range of light intensity used in our experiments is not large enough to reach the saturation point.

For n-type and undoped GaN materials, the dependence of the etching rate on light intensity shows the similar trend (Figures 4.1(b) and 4.9). With the increase in the light intensity, etching rates increases monotonically as higher light intensities will generate a larger number of holes. Consequently, the variation in the light intensity will allow us to elucidate on the effects of these generated holes on the etching process. The effects of the solution concentration on the etching rates are a little more complicated (Figures 4.1(a) and 4.8). At low concentrations, there is a short supply of OH^- ions; hence the removal of surface oxides becomes the rate-limiting process. At high concentrations, the number of generated holes may be deficient at the fixed light intensity and the ratio between the numbers of free water molecules to solute ions is reduced. Therefore the rate of oxide formation then becomes a limiting factor in the etching process. The etching rate falls off dramatically at high concentrations in the experiments for undoped GaN when the concentration of KOH solution is more than 0.1M. Similar results have also been presented in other reports [25,76]. The reason is most likely due to the effects of water molecules in the etching process. The existence of water molecule plays an important role in the dissolution of gallium oxide to form the gallium oxide ions. The gallium oxide ions could not been effectively dissolved in the limited water molecule, which make the etching slow due to the residual gallium oxide layer on the sample and form an uncontinuous layer to rough the etched surface.

Peng *et al.* [18] showed that no PEC wet etching was observed in solutions of KOH dissolved in ethanol to clarify the important role of H_2O solvent in the PEC wet etching of GaN. The exact mechanism of water molecules in the mixture of KOH and $K_2S_2O_8$ solution for ELPEC wet etching needs further investigations.

The surface morphology depends upon both the crystallographic and chemical nature of the defects, which often assumes a complex shape. Figure 4.3 shows the evolution of several different sets of surface morphology obtained in different etching conditions as a function of the concentration of the solution. A smoothly etched surface would indicate uniform oxidation reaction throughout the surface of the sample, with negligible repulsion or recombination occurring at the defects, or dislocations. The dislocation etching morphology is characterized by the formation of small whiskers due to the rapid nonradiative recombination effects at the dislocations. The dislocations may introduce recombination centres due to the presence of crystal defects in the material. The trapping phenomenon will result in the local reduction in the concentration of holes on the surface. Figure 4.3(a) shows the initial breakdown of the smooth surface as selective etching begins to occur around dislocations, which is called intermediate morphology in the surface evolution. The columnar nanostructure etch morphology (shown in Figure 4.3(b)) consists of dense whisker formations. This morphology is the characteristic etched surface when using a solution with an intermediate concentration as opposed to a smooth and dislocation-free surface morphology. This would indicate a less dissolution-limited etch process, resulting in a higher etching rate around the dislocations leading to the formation of dense whiskers.

In Figure 4.3(c), the dense whisker formations from the previous morphology have broken down, and the surface has evolved into a series of cellular pits. This is characteristic of wet etching performed at high pH levels. During the etching process at these conditions, the etching rate between dislocations is increased further, resulting in the development of pits between dislocations and the formation of a relatively flat surface.

The mechanism of the smooth photoenhanced etching of GaN appears to be related to the dissolution-limited etching conditions [77]. It is indicated that smooth etching occurs with low solution concentration or high light intensity, consistent with the observed results in Figure 4.8 and Figure 4.9. In lower concentrations of KOH solution, since the oxide is not dissolved rapidly, the residual oxide acts as a spacer layer to separate unetched GaN from the electrolyte. Although the residual oxide at the GaN surface impedes further etching, this layer can assist in maintaining a smooth etched surface by counteracting selective etching between crystalline GaN and defected/dislocated GaN caused by the nonuniform distribution of holes at the surface. The turning point of dissolution-limited reaction is determined, in part, by the particular illumination condition. In our case for undoped GaN etching by ELPEC technique, at the light intensity of 1.68W/cm^2, the turning point is around the pH value of 12.8. Below this value, local variations in the surface reactivity due to material defects are no longer significant. As in the case of higher light intensities, a higher concentration of holes is induced on the GaN surface, leading to an increased etching rate while also supplying additional holes to regions where holes are depleted

by defect-induced recombination. This results in a more uniform spatial distribution of holes, and results in a more smoothly etched surface. However, when etching is conducted in high solution concentrations or at low light intensities, the rough morphology easily occurs at defects and dislocations. That is why the corresponding RMS roughness in these cases are high.

Considering that the concentration of the solution influences both the etching rate and surface morphology of etched samples, although smooth surfaces can be obtained in a low concentration solution for n-type GaN materials, the concentration of KOH solution cannot be too low for applications in large area mesa etching. Besides the low etching rate in the low concentration solution, according to the results obtained from experiments on the effect of sample geometry in different concentrations of the solution, one observes significant changes in the etching rate as moving away from the metal mask. Regions close to the mask showed enhanced etching rates as compared to most regions that showed lower etching rates. Except for the reason of the inadequate convection of liquid, this phenomenon also can be caused by the band bending in the semiconductor at the GaN/metal interface. The interface between intrinsic GaN and the metal mask is similar to the interface of intrinsic GaN/KOH solution shown in Figure 2.3. In a way, the sample-edge portion, which is near the metal region, is an area in which it is easier for the carriers to move. If holes exist in higher concentration at the metal/semiconductor interface, the edges of the exposed regions etch at such a greater rate than the centre of the region that they effectively isolate the exposed regions very quickly. This type of accelerated etching near the

metal mask was also observed in both electrode and electrodeless PEC wet etching by others [22,30,78]. Similar results are also observed in our experiments for undoped GaN as seen in Figure 4.6. Depending on the lifetime and diffusion characteristics of the photo-generated carriers, holes generated at an appreciable distance away from the edge of a pattern may diffuse to the feature perimeter and enable an enhanced localized etching rate. At the regions close to the metal mask, there is an abundant supply of carriers. This phenomenon is particularly obvious in the experiments for the etching of undoped GaN, with a positive bias applied. If a positive bias is applied to the GaN film, the chemical potential of the surface is reduced, which flattens the bands. Then a higher concentration of holes will accumulate at the interface and improve the etching process. Therefore, if the bands are sufficiently flattened, photoenhanced etching may occur due to the photo-carriers generated near the surface, as reported by J. E. Borton *et al.* [27]. That is, the etching rate is strongly dependent on the chemical potential of the surface.

Moreover, in our experiments, it is found that the post-treatment method with ultrasonic agitation in hot KOH is the most efficient way to smooth the etched surface. After etching, some samples were treated with ultrasonic in 60℃ 2M KOH for 10 minutes. Figure 4.11 reveals the amelioration in surface roughness as SEM images shown. The same phenomenon also occurred in the etching process under other conditions. Especially for a rough etched surface, post-treatment seems to be more helpful. The two images in Figure 5.1 show the typical changes due to the effect of ultrasonic treatment. The experiment was conducted in a mixture of 0.5M KOH and

0.05M $K_2S_2O_8$ at the light intensity of 1.68W/cm^2. Figure 5.1(a) shows the SEM image of the etched surface before ultrasonic treatment, with an RMS roughness of 38.763nm. Figure 5.1(b) shows the marked difference in the SEM image of the same etched surface after ultrasonic treatment, with an RMS roughness of 16.469nm. It seems that much of the whiskers are physically broken off by solution agitation during ultrasonic treatment forming a substantially smoother surface. Even in the smoothest case of etching in 0.01MKOH+0.05M$K_2S_2O_8$ solution, the roughness was reduced from 10.527nm to 6.427nm. Our results show that ultrasonic treatment in hot KOH really plays a potentially important role in the device processing because of the smoother etched surface it can produce.

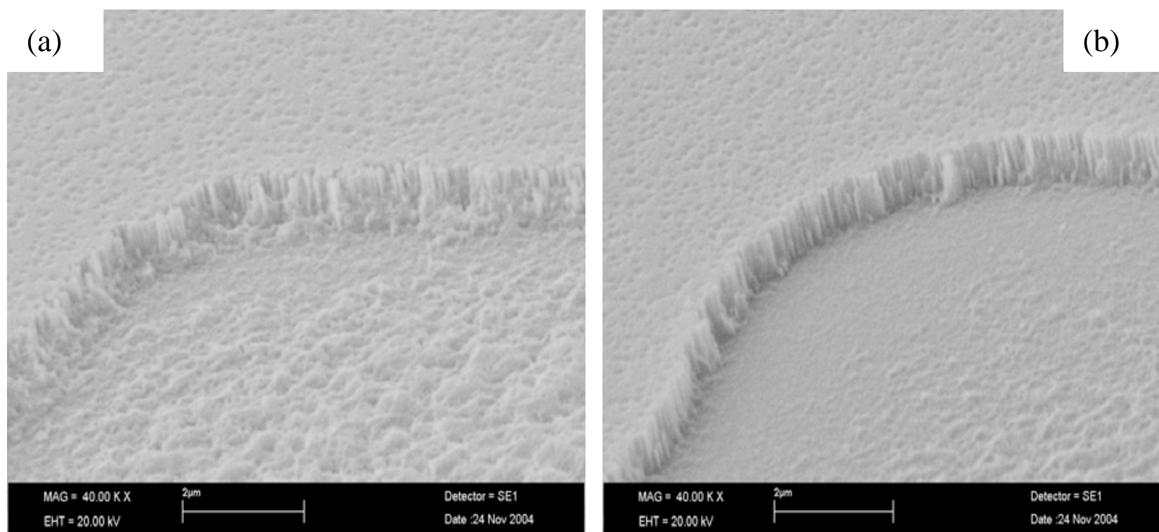

Figure 5.1 Ultrasonic treatments in 2M KOH solution at 60℃ for10 minutes

Etching rate and surface morphology as two important standards to evaluate the etching process are widely applied. As shown in Figure 4.8, although the RMS roughness for the etched surface in the 0.01M KOH solution is a little smoother than

the rest, the etching rate is about two times slower than that obtained in the 0.1M KOH solution. Hence, even in the mixture of 0.01M KOH and 0.05M $K_2S_2O_8$, the etched surface is the smoothest one. But this condition is not suitable for the application of mesa etching because of the low etching rate. As a trade-off between etching rate and surface morphology, the optimum solution concentration for etching undoped AlGaN/GaN heterostructure mesa etching is a mixture of 0.1M KOH and 0.05M $K_2S_2O_8$ in proportion of 1:1 and the optimum light intensity is 1.68W/cm^2. However, the influence of surface morphology on practical application is not concretely explored yet, though the key objective is to obtain a very smooth surface with a high etching rate. Therefore, in this thesis a systematic study on a series of samples fabricated on undoped AlGaN/GaN heterostructure with cross-bridge structures in various etching conditions is investigated. The corresponding electrical properties are discussed below.

First, Hall Effect measurement was examined as a means to characterize the transport properties of charge carriers in the semiconductor materials. Figure 4.13 shows the typical mobility and sheet carrier concentration of 2D electrons as a function of temperature. The carrier density with temperature is nearly constant, which confirms that no parasitic conduction occurs through the undoped material. Normally, for bulk GaN materials, the dependence of the Hall mobility on temperature has a maximum point at nearly 200K [82-84]. The monotonic increase in the mobility with decreasing temperature is an indication of the presence of a 2DEG. The variations of the mobility between samples of different etching conditions

may be attributed to interface roughness at AlGaN/GaN interface as well as the roughness and the trap density at the sidewalls. Figure 4.14 illustrates the mobilities tested at room temperature as a function of the concentration of the solution and light intensity. Comparing Figure 4.14 with Figures 4.8 and 4.9, it is clear that a relationship exists between mobility and the roughness of the etched surface. The smoother the surface, the higher is the corresponding mobility. The possible reason to explain this phenomenon is that the etching condition affects the roughness at the sidewalls of the etched structure. The rougher the sidewall, the more defects may exist. In addition, the surface roughness will influence the density of dangling bonds and scattering in the samples. Higher surface roughness will result in the increased density in the dangling bonds leading to the increase in the trapping and detrapping of the carriers by the surfaces states and the scattering of carriers by the defect states. This results in the increase in the low-frequency noise power spectral density and the reduction in carrier mobility. This agrees with the results by Dang *et al*. [75] who showed that for low carrier concentration, the reduced dependence of mobility on temperature suggested scattering by dislocations and defects is more significant. Consequently the Hall mobilities obtained from different devices may be used as an indication of the density crystalline defects in the materials. Combined with the experimental results, it may be concluded that ELPEC wet etching would induce some material defects during the etching process. To further investigate the relationship between the etching conditions of the samples and the corresponding

performance of the devices we investigated the low-frequency noise properties of the heterostructures.

In Figure 4.15, the noise levels of these nine samples appear very different. However, combined with the corresponding results on surface roughness, it is discovered that the variation of noise level is consistent with the corresponding changes of surface roughness: the rougher the surface is, the higher the level of low-frequency noise, which also represents the same trend as the relationship between mobility and surface roughness as analyzed above. The room temperature Hooge parameters calculated from the typical experimental results using ELPEC and conventional ICP etching techniques, based on Eq. (2.2.12), are shown in Table 5.1:

Table 5.1

Device	**Concentration of the solution**	**Light intensity**	**Hooge Parameter**
A	0.01M KOH + 0.05M $K_2S_2O_8$	1.68 W/cm^2	1.9×10^{-3}
B	0.05M KOH + 0.05M $K_2S_2O_8$	1.68 W/cm^2	2.0×10^{-3}
C	0.1M KOH + 0.05M $K_2S_2O_8$	1.68 W/cm^2	2.2×10^{-3}
D	0.2M KOH + 0.05M $K_2S_2O_8$	1.68 W/cm^2	6.7×10^{-3}
E	0.5M KOH + 0.05M $K_2S_2O_8$	1.68 W/cm^2	7.6×10^{-3}
F	0.1M KOH + 0.05M $K_2S_2O_8$	1.36 W/cm^2	6.9×10^{-3}
G	0.1M KOH + 0.05M $K_2S_2O_8$	1.04 W/cm^2	8.7×10^{-2}
H	0.1M KOH + 0.05M $K_2S_2O_8$	0.80 W/cm^2	1.7×10^{-2}
J	0.1M KOH + 0.05M $K_2S_2O_8$	0.64 W/cm^2	1.2×10^{-2}
K	*ICP etching*		9.1×10^{-3}

The level of low-frequency noise and the corresponding value of Hooge parameter are strongly depend on the growth technique and the different types of substrates [71, 85-89]. The Hooge parameter is directly proportional to the trap density. Thus, a smaller Hooge parameter stipulates low defect density of the material. It is not surprising that devices which exhibit lower Hooge parameters also demonstrate higher electron mobility. The results of the comparison between ELPEC wet etching and ICP dry etching techniques are shown in Figure 4.19 and Figure 4.20. The results demonstrate that the low-frequency excess noise level of devices fabricated under the optimal ELPEC etching condition is about half an order of magnitude lower than the devices fabricated by the ICP dry etching technique, with a Hooge parameter of 2.2×10^{-3} at room temperature. This value is less than the most reported results obtained from the samples grown on sapphire structure by MBE technique. The higher electron mobility and the lower noise level of devices fabricated by ELPEC wet etching point out that this technique indeed causes less damage during the etching process and may find potential applications in the fabrication of GaN-based devices.

It is well known that low-frequency excess noise is not only an important figure-of-merit for electronic and optoelectronic devices, but also a powerful tool for the characterization of defect states in materials. The noise voltage power spectral density of the occupancy of the traps is given by the following expression [90]:

$$S_V(f) = 4I^2(\Delta R)^2 \int_x \int_y \int_z \int_E N_T(x,y,z,E) \times \frac{\tau}{1+4\pi^2 f^2 \tau^2} dxdydzdE, \quad (5.1.1)$$

in which I is the *dc* current bias applied to the device, ΔR is the resistance fluctuation caused by the capture or emission of a single electron by a defect, N_T is the defect density in the materials and τ is the fluctuation time constant. At room temperature, the observed noise is close to typical *1/f* noise in our experiments. However, noise measurement at low temperature can reveal the contribution of very shallow trap levels. Noise data for the purpose of noise spectroscopy are usually represented in the form of ($S_V(f) \times f$) versus f at different temperatures as shown in Figure 4.18. In this case, the temperature dependence $S_V(f) \times f$, directly yields time constant $\tau = 1/2\pi f_0$ and its temperature dependence (here f_0 is the characteristic frequency of the G-R spectrum). Plotting of ln $(T^2\tau)$ against $1/T$ in Figure 5.2 yields the only one activation energy at 86.2 meV. The concentration of G-R centre can be determined from Eq. (2.2.17). Analyses of S_0 show that its temperature dependence is mainly determined by the Fermi factor $f_T(1-f_T)$, at $E_T = E_F$ it is found that [93]

$$f_T(1-f_T)\big|_{E_F=E_T} = 1/4, \qquad \text{and} \tag{5.5.2}$$

$$S_{0\max} = \frac{V^2}{N^2} N_T A\,. \tag{5.5.3}$$

Equation 5.5.3 assumes that the trapping and detrapping process results in the modulation of carrier density at the vicinity of the localized states. Figure 5.3 shows the temperature dependence of S_0 and from the maximum S_0, and the sheet trap density is calculated with the value of 5.45×10^{13} cm^{-2} by assuming number fluctuation model. S. L. Rumyantsev *et al.* [91-92] suggested that G-R noise for GaN heterostructures

cannot be located directly in the two-dimension electron gas. Also, the observed G-R noise cannot be explained by the tunnelling of electrons from the two-dimension channel to GaN or AlGaN, because this process is not thermally activated and should show little dependence on the device temperature. The possible locations for G-R centres are in the AlGaN barrier layer or in the undoped GaN layer. In our case, the calculated activation energy of 86.2 meV has been reported in the past for rf-plasma assisted MBE-grown GaN films [66, 94]. It is, therefore, reasonable to speculate that the G-R centres are located in the undoped GaN layer.

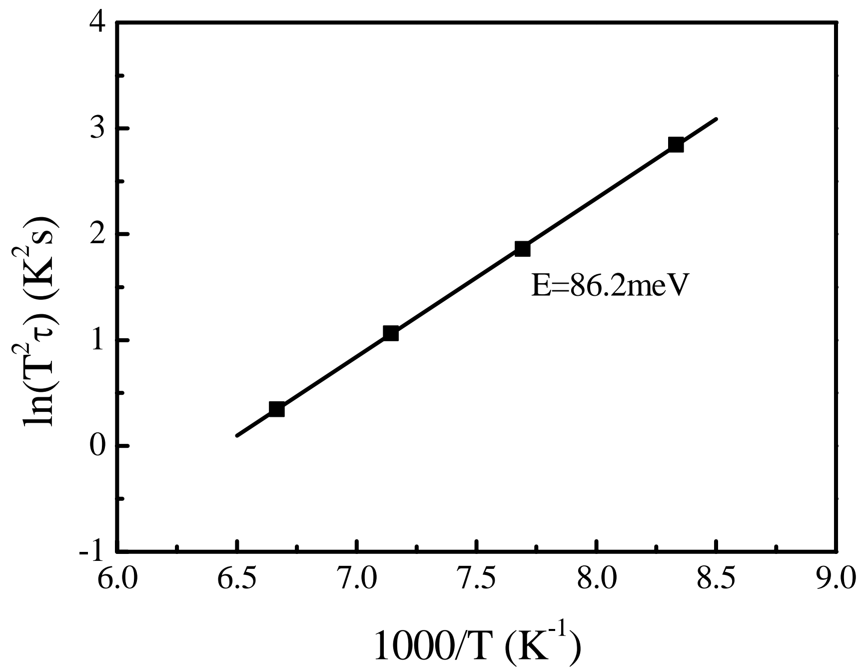

Figure 5.2 Arrhenius plots of the fluctuation time constant τ.

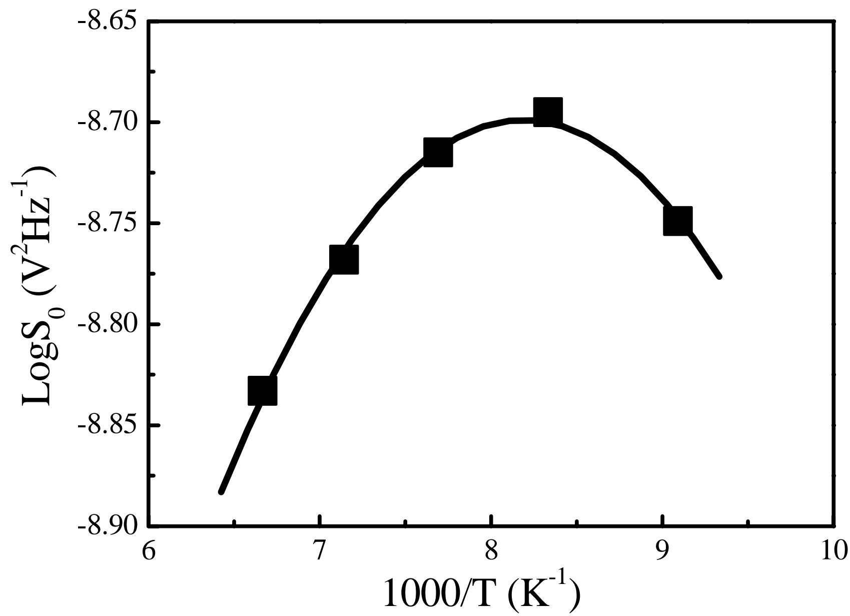

Figure 5.3 Low temperature G-R noise magnitude $\log_{10}(S_0)$ is plotted as a function of temperature

The experimental results on low temperature noise measurement reveal that G-R noise is not dominant in our samples. Even at low temperatures, the amplitude of *1/f* noise is preponderant in samples C, E, and H. In this case, the typical temperature dependences of $S_V(f)$ are illustrated in Figure 4.17. Base on the above Eq.(2.2.20), and calibrate the value from the above calculated sheet trap density. The trap density can be obtained varied with the trap energy. The experimental data on the sheet trap densities for samples C, E, H and those fabricated by ELPEC wet etching and ICP dry etching versus activation energy are shown in Figure 5.4. We observe that the trap density in the AlGaN/GaN heterostructure is significantly affected by the fabrication process. The results also show that the corresponding trap density in devices fabricated by ELPEC wet etching is lower, which clearly indicates that the ELPEC

technique may lead to lower material damage induced during the etching process compared with ICP dry etching.

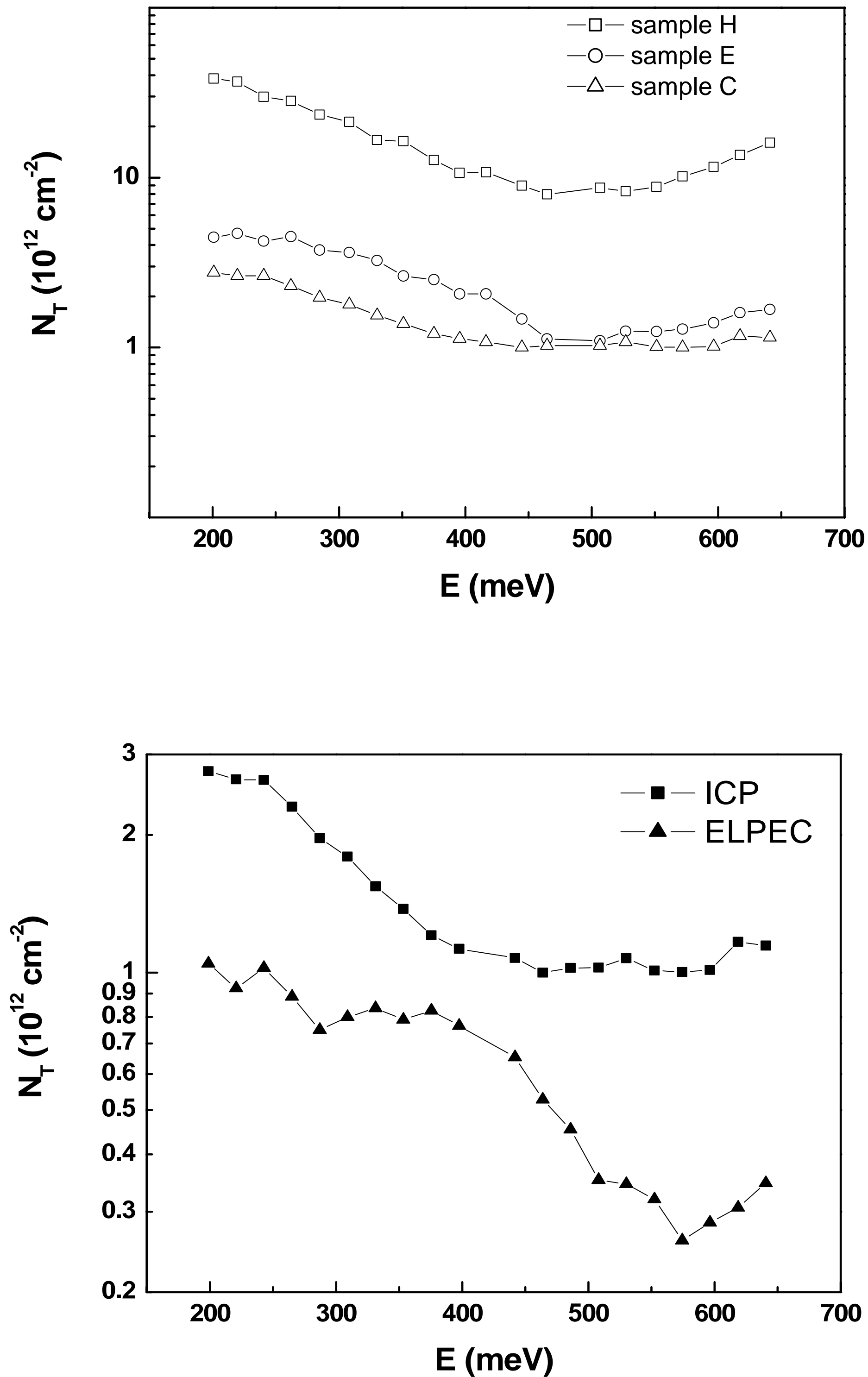

Figure 5.4 Typical results illustrating the sheet trap density in samples

Chapter 6. Conclusions and Directions for Future Work

The present study focuses on the fabrication and characterization of GaN-based materials by PEC wet etching technique that offers the key advantages of less induced damage, high etching selectivity and low cost implementation. We have successfully etched n-type GaN, undoped GaN and undoped AlGaN/GaN heterostructure by PEC wet etching techniques. The morphological and electronic properties of the devices are examined in detailed. The mechanism of PEC wet etching is reviewed extensively. The systematic investigations on the characteristics of electrode PEC wet etching has been conducted on a wide variety of conditions for n-type GaN samples. The results provide us with insights on the optimal experimental setup and etching conditions. Moreover, the effects of light intensity, concentration of the solution and external biasing on the experimental results are helpful to the across-the-board understanding of the reaction mechanism. For n-type GaN, the maximum etching rate is 83nm/min under $30mW/cm^2$ light intensity in 0.1M KOH solution with $33mA/cm^2$ current density applied.

For undoped GaN, it is difficult to realize the total isolation of mesa structure at the same condition as electrode PEC wet etching for n-type GaN. Only the region near the metal mask is etched because of high resistance of the film itself. In this case, the lack of holes at the reaction interface of undoped GaN/solution is supplied by the addition of $K_2S_2O_8$ in the solution, which can generate a hole, and ELPEC technique replaces the one with electrode to attain mesa structure. Light intensity and

concentration of the solution are two of the important etching parameters discussed. As a trade-off between etching rate and surface morphology, it is found that the optimal concentration of the etching solution consists of 0.1M KOH: 0.05M $K_2S_2O_8$ in proportion of 1:1. The film was etched under the illumination of the He-Cd laser at the light intensity of 1.68W/cm^2. The maximum etching rate is about 22nm/min and RMS roughness of the etched surface is 17.379nm. The smoothest surface was obtained in the mixture solution of 0.01M KOH and 0.05M $K_2S_2O_8$ with etching rate of 12nm/min and RMS roughness of 10.527nm, which is smoother than the RMS roughness 11.469nm of as-grown films. In addition, the post-treatment method with ultrasonic agitation in hot KOH is an efficient method to improve the surface roughness. If the samples are treated with ultrasonic in 60℃ 2M KOH for 10 minutes after etching, the roughness of etched surface is further improved.

To investigate the effects of PEC wet etching on the electronic properties of the films, we fabricated cross-bridge $Al_{0.13}Ga_{0.87}N$/GaN heterostructure under different etching conditions with ultrasonic treatment. Hall mobility and low-frequency excess noise as the main characteristics of cross-bridge structures being examined. The experimental results show that the Hall mobilities at room temperature and low-frequency excess noise levels of the devices fabricated under different conditions are consistent with the corresponding changes of surface roughness. A Lorentzian bump originating from the generation-recombination process is observed at low temperature range and its thermal activation energy is about 86.2meV. Furthermore, by comparing the characteristics of devices fabricated by ELPEC technique with

those obtained by ICP dry etching, it is obvious that the electrical properties of ELPEC etched device are better. The low-frequency excess noise level of devices fabricated by optimal PEC etching condition, with a room temperature Hooge parameter of 2×10^{-3}, is about half of an order lower than that of devices fabricated by ICP dry etching technique, which has a typical value of 9×10^{-3}. The experiments demonstrate that PEC wet etching is a better and simpler way to fabricate GaN devices with high quality and good performances, and is well adapted to the future development of device fabrication on GaN materials.

This project has both academic value and practical significance. Nowadays, the important application of PEC wet etching exists in recessed gate etching on GaN-HEMTs for high-quality AlGaN/GaN heterostructures [95-97]. Ideally, if PEC wet etching technique is utilized for both mesa structure and recessed gates, the devices would have better properties. In most cases, low etching rates of PEC wet etching blocked the development of mesa etching, especially for undoped GaN based materials. The ability to etch both undoped and p-type GaN is the most important advantage of ICP dry etching. However, it is known that the technique may quite a significant amount of crystalline damage at the etched surface. Our experiments provide a feasible and repeatable method to achieve mesa etching for undoped films that can be widely applied in practical device fabrication to achieve better performance. Future work includes the application of this technique on the fabrication practical electronic and optoelectronic devices such as GaN HEMTs and LEDs.

References

1. **S. J. Pearton, J. C. Zolper, R. J. Shul and F. Ren, "**GaN: Processing, Defects, and Devices", *J. Appl. Phys. Vol. 86, No.1, 1-78,* 1999
2. **S. Yoshida, S. Misawa, and S. Gonda, "**Epitaxial growth of GaN/AlN heterostructures**",** *J. Vac. Sci. Technol.B1, 250,*1983
3. **I. Akasaki and H. Amano,** "Heteroepitaxial growth and the effects of strain on the luminescent properties of GaN films on (11&twobar;0) and (0001) sapphire substrates", *Jpn. J. Appl. Phys. 27,L1384,*1988
4. **I. Akasaki, H. Amano, Y. Koide, K. Hiramatsu, and N. Sawaki, "**Effects of ain buffer layer on crystallographic structure and on electrical and optical properties of GaN and $Ga_{1-x}Al_xN$ ($0 < x \leqq 0.4$) films grown on sapphire substrate by MOVPE", *J. Cryst. Growth 98, 209,*1989
5. **T. L. Tansley and R. J. Egan, "**Point-defect energies in the nitrides of aluminum, gallium, and indium", *Phys. Rev. B 45, 10942,* 1992
6. **Fong, Wai keung, "**Growth of High Quality Gallium Nitride Thin Films by RF-Plasma assisted MBE", *Thesis Report in The Hong Kong Polytechnic University,* 2001
7. **Randy J. Shul, "**Inductively Coupled Plasma Etching of Ⅲ−Ⅴ Nitrides", *Sandia National Laboratories, NM87185-0603,USA*
8. **I. Adesida, A. Mahajan, E. Andideh, M. Asif Khan, and D. T. Olsen,** "Reactive ion etching of gallium nitride in silicon tetrachloride plasmas"**,** *Appl. Phys. Lett., 63, 2777*, 1993
9. **L. Zhang, J. Ramer, K. Zheng, L. F. Lester and S. D. Hersee, "**Electron cyclotron resonance etching characteristics of GaN in $SiCl_4$/Ar", *Appl. Phys. Lett. 68, 367,* 1996
10. **I. Adesida, A. T. Ping, C. Youtsey, T. Snow, M. Asif Khan, D. T. Olson, and J. N. Kuznia, "**Characteristics of chemically assisted ion beam etching of gallium nitride", *Appl. Phys. Lett. 65, 889,* 1994

11. **R. J. Shul, G. B. McClellan, S. A. Casalnuovo, D. J. Rieger, S. J. Pearton, C. Constantine, C. Barratt, R. F. Karlicek, Jr., C. Tran, and M. Schurman,** **"**Inductively coupled plasma etching of GaN"**,** *Appl. Phys. Lett. 69, 1119,* 1996
12. **Jack Huynh, Newton Cheng, and Jerry Hitchcock, "**Photoelectrochemical Wet Etching of Gallium Nitride", 2000
13. **S. Strite and H. Morkoc, "**GaN, AlN, and InN: A review"**,** *J. Vac. Sci. Technol. B 10, 1237,* 1992
14. **S. J. Pearton, C.R. Abernathy, F. Ren, J. R. Lothian, P.W. Wisk, and A. Katz, "**Dry and wet etching characteristics of InN, AlN, and GaN deposited by electron cyclotron resonance metalorganic molecular beam epitaxy**",** *J. Vac. Sci. Technol. A 11,1772,* 1993
15. **B. J. Kim, J. W. Lee, H. S. Park, Y. Park, and T. I. Kim, "**Wet Etching of (0001) GaN/(Al_2O_3) Grown by MOVPE", *J. Electron. Mat. 27, L32,* 1998
16. **D. A. Stocker, E. F. Schubert, and J. M. Redwing, "**Crystallographic Wet Chemical Etching of GaN", *Appl. Phys. Lett. Vol 73, 2654,*1998
17. **M. S. Minsky, M. White, and E. L. Hu, "**Room- temperature photoenhanced wet etching of GaN", *Appl. Phys. Lett. 68, 1531,* 1996
18. **L.-H. Peng, C.-W. Chuang, J.-K. Ho, C.-N. Huang and C.-Y. Chen, "**Deep Ultraviolet Enhanced Wet Chemical Etching of Gallium Nitride", *Appl. Phys. Lett. Vol. 72, No. 8, 939-941,* 1998
19. **Seikoh Yoshida, "**Electrochemical Etching of a Conductive GaN Crystal for Patterning", *J. Crystal Growth 181, 293-296,* 1997
20. **P. Visconti, M. A. Reshchikov, K. M. Jones, F. Yun, D. F. Wang, R. Cingolani and H. Morkoç**, **"**Highly Selective photoenhanced Wet Etching of GaN for Defect Investigation and Device Fabrication", *Virginia Commonwealth University, Dept. of Electrical Engineering, Richmond, VA, 23284*
21. **H. Q. Lu, Z. Wu, and I. Bhat,** "Photoassisted Anodic Etching of Gallium Nitride", *J. Electrochem. Soc. 144, No.1, L8-L11,* 1997
22. **C. Youtsey, I. Adesida, L. T. Romano, and G. Bulman, "**Smooth n-type GaN surfaces by photoenhanced wet etching", *Appl. Phys. Lett. 72, 560,* 1998

23. **C. Youtsey, L. T. Romano, and I. Adesida, "**Gallium nitride whiskers formed by selective photoenhanced wet etching of dislocations", *Appl. Phys. Lett. 73, 797,* 1998
24. **C. Youtsey, G. Bulman, and I. Adesida, "**Dopant-selective Photoenhanced Wet Etching of GaN", *J. Electron. Mater. 27, 282,* 1998
25. **Hyun Cho, S. M. Donovan, C. R. Abernathy, S. J. Peartno, F. Ren, J. Han and R. J. Shul,** "Photoelectrochemical etching of $In_xGa_{1-x}N$", *MRS Internet J. Nitride Semicond. Res. 4S1, G6.40,* 1999
26. **Mitsugu Ohkubo,** "Photo-assisted anodic etching of GaN films in NaOH electrolyte with Cl ions"**,** *Materials Science and Engineering B, Vol.59, 355-357,* 1999
27. **J. E. Borton, C.Cai, M. I. Nathan, P. Chow, J. M. Van Hove, A. Wowchak, and H. Morkoc, "**Bias-assisted photoelectrochemical etching of p-GaN at 300 K", *Appl. Phys. Lett. Vol.77, No.8,* 2000
28. **J. M. Hwang, K. Y. Ho, Z. H. Hwang, W. H. Hung, Kei May Lau, and H. -L. Hwang,** "Efficient wet etching of GaN and p-GaN assisted with chopped UV source", *Superlattices and Microstrcture, 1-13,* 2004
29. **J. A. Bardwell, I. G. Foulds, J. B. Webb, H. Tang, J. Fraser, S. Moisa, and S. J. Rolfe, "**A simple wet etch for GaN", *J. Electron. Mater. 28, L24,* 1999
30. **J. A. Bardwell, I. G. Foulds, B. Lamontagne, H. Tang, J. B. Webb, P. Marshall, S. J. Rolfe, J. Stapleton, and T.W. MacElwee,** "Fabrication of high performance GaN modulation doped field effect transistors", *J. Vac. Sci. Technol. A 18, 750-753,* 2000
31. **H. Maher, D. W. Disanto, G. Soerensen, C. R. Bolognesi, H. Tang, and J. B. Webb, "**Smooth wet etching by ultraviolet-assisted photoetching and its application to the fabrication of AlGaN/GaN heterostructure field-effect transistors", *Appl. Phys. Lett. Vol. 77, No.23, 3822-3835,* 2000
32. **P. A. Kohl, "**Photoelectrochemical Etching of Semiconductors", *Electrochemical Microfabrication Vol. 42, No.5*, 1998

33. **M. Balkanski and R. F. Wallis, "**Semiconductor Physics and Applications", *Oxford University press*

34. **Holger T. Grahn, "**Semiconductor Physics", *World Scientific*

35. **E. Liu, B. Zhu, and J. Luo, "**Semiconductor Physics", *House of Electronics Industry, Beijing,* 2003

36. **J. Hladik, "**Physics of Electrolytes", *Academic Press*

37. **H. Gerischer, "**Physical Chemistry", *Academic Plenum Press*

38. **S. R. Morrison, "**Electrochemistry at Semiconductor and Oxidized Metal Electrodes", *Plenum Press*

39. **K. Sangwal, "**Etching of Crystals: Theory, Experiment, and Application", *Elsevier Science Publishers B.V., Amsterdam,* 1987

40. **Christopher T. Youtsey, "**Photoelectrochemical Wet Etching of Gallium Nitride", *University of Illinois at Urbana-Champaign,* 1999

41. **P. H. L. Notten, J. E. A. M. van den Meerakker, and J. J. Kelly, "**Etching of III-V semiconductors: An Electrochemical Approach", *Elsevier Science, Amsterdam,* 1991

42. **C. Youtsey, I. Adesida and G. Bulman, "**Highly anisotropic photoenhanced wet etching of n-type GaN", *Appl. Phys. Lett. 71, 2151,* 1997

43. **D.J. O'Connor, B.A. Sexton, and R.St.C. Smart, "**Surface Analysis Methods in Materials Science", *Springer, Physics and Astronomy,*2003

44. **John C. Vickerman, "**Surface Analysis-The Principal Techniques", *John Wiley & Sons,*1997

45. **J. Gao, "**SEM and TEM Laboratory Report", *The Hong Kong Polytechinc University,*2004

46. **J. Gao, "**STM and AFM Laboratory Report", *The Hong Kong Polytechinc University,*2004

47. **NT-MDT,** "Solver P47 SPM Instrution Manual", http://www.ntmdt.ru

48. **Scanning Probe Microscopy at Bristol, "**Atomic Force Microscopy", http://spm.phy.bris.ac.uk/techniques/AFM/

49. **J.O. Bird, "**Engineering mathematics", *Oxford, Butterworth-Heinemann*,1996

50. **R S Popovic, "**Hall Effect Devices", *The Adam Hilger Series on Sensors,*1991
51. "The Hall Effect",
http://class.phys.psu.edu/p559/experiments/html/hall_effect_2004.htm
52. **Van Zeghbroeck**, "Principle of Semiconductor Devices", 2004
53. **Y. Q. Lee, "**Temperature-dependant Hall Measurement on Undoped GaN" Epilayer, *National Sun Yat-sen University, Taiwan,*1993
54. "HL5500PC Operator's Manual Issue"
55. "Semiconductor Electronics Division",
http://www.eeel.nist.gov/812/effe.htm#lore
56. "Hall Measurement", *the laboratory report in Drexel University,U.S.*
57. **Sze Him Ng, "**Low-Frequency Excess Noise in Resonant Tunneling Diodes", *Northeastern University,* April, 1993
58. **P.J.Fish,** "Electronic Noise and Low Noise Design", *Houndmills, Basingstoke ; London : Macmillan*, 1993
59. **Dai Yisong, "**Zao Sheng Dian Zi Xue", *Shandong ke xue ji shu chu ban she*, 1997
60. **Andras Ambrozy**, "Electronic Noise", *McGraw-Hill International Book Co.*, 1982
61. **Sh Kogan, "**Electronic noise and fluctuations in solids"**,** *Cambridge University Press*, 1996
62. **Fazal Ali, Aditya Gupta, "**HEMTs and HBTS: Devices, Fabrication, and Circuits", *Artech House, Boston London,* 1991
63. **F. N. Hooge, T.G. M. Kleinpenning, and L.K.J. Vandamme, "**Experimental studies of *1/f* noise**",** *Rep. Prog. Phys., Vol.44, pp.479-532,* 1981
64. **P.`H.`Handel,** *Phys. Rev. Lett., vol.34, 1492,* 1975
65. **S. Machlup,** *J. Appl. Phys. No.25, pp.341*, 1954
66. **B.H. Leung, W.K. Fong, C.F. Zhu, and C. Surya, "**Low-frequency noise in GaN thin films deposited by rf-plasma assisted molecular-beam epitaxy", *Appl. Phys. Lett., Vol.91, No.6, pp.3706-3710,* 2002

67. **Shawn S.H. Hsu, Pouya Valizadeh, Dimitris Pavlidis,** "Characterization and Analysis of Gate and Drain Low-frequency Noise in AlGaN/GaN HEMTs", *The university of Michigan, USA,*2002

68. **W.K. Fong, C.F. Zhu, B.H. Leung, and C. Surya, "**High-mobility GaN epilayer grown RF plasma-assisted molecular beam epitaxy on intermediate-temperature GaN buffer layer"**,** *Journal of Crystal Growth, No.233, pp. 431-438,* 2001

69. **Z.H. Feng, Y.D. Qi, Z.D. Lu, and K.M. Lau,** *Journal of Crystal Growth, 272(1-4):327-332,*2004

70. **C. Youtsey, "**Photoelectrochemical Etching of Gallium Nitride", *Thesis report in University of Illinois* , 1999

71. **M.E. Levinshtein, F. Pascal, S. Contreras, W. Knap, S.L. Rumyantsev, R. Gaska, J.W. Yang, and M.S. Shur, "**AlGaN/GaN high electron mobility field effect transistors with low *1/f* noise", *Appl. Phys. Lett., Vol.72, No.23, pp.3053-3055,* 1998

72. **Z. H. Hwang, J. M. Hwang, W. H. Hung, and H. L. Hwang, "**Electrodeless wet etching of GaN assisted with chopped ultraviolet light", *Appl. Phys. Lett., Vol.84, No.19, pp.3759-3761,* 2004

73. **Chao-Yi Fang, Weng-Jung Huang, Edward Yi Chang, Chia-Feng Lin, and Ming-Shiann Feng, "**Etching Damages on AlGaN, GaN and InGaN Caused by Hydrid Inductively Coupled Plasma Etch and Photoenhanced Chemical Wet Etch by Schottky Contact Characterizations", *Jpn. J. Appl. Phys., Vol.42, pp.4207-4212,* 2003

74. **R. Oberhuber, G. Zandler, and P. Vogl, "**Mobility of two-dimensional electrons in AlGaN/GaN modulation-doped field-effect transistors", *Appl. Phys. Lett., Vol.73, No.6, pp.818-820,* 1998

75. **X.Z. Dang, P.M. Asbeck, E.T.Yu, G.J. Sullivan, M.Y. Chen, B.T. McDermott, K.S. Boutros, and J.M. Redwing, "**Measurement of drift mobility in AlGaN/GaN heterostructure field-effect transistor", *Appl. Phys. Lett., Vol.74, No.25, pp.3890-3892,* 1999

76. **Y.K. Su, S.J. Chang, T.M. Kuan, C.H. Ko, J.B. Webb, W.H. Lan, Y.T. Cherng, and S.C. Chen, "**Nitride-based Schottky diodes and HFETs fabricated by photo-enhanced chemical wet etching", *Mat. Sci.& Eng.B Vol. 110, pp.260-264*, 2004
77. **Bo Yang, and Patrick Fay, "**Etch rate and surface morphology control in photoelectrochemical etching of GaN", *J. Vac. Sci. Technol. B 22(4), pp.1750-1754,* 2004
78. **E Harush, S Brandon, J Salzman, and Y Paz,** "The effect of mass transfer on the photoelectrochemical etching of GaN", *Semicond. Sci. Technol. 17, No.6, pp.510-514,* 2002
79. **J. A. Bardwell, J. B. Webb, H. Tang, J. Fraser, and S. Moisa,** "Ultraviolet photoenhanced wet etching of GaN in $K_2S_2O_8$ solution", *J. Appl. Phys. Vol.89, No.7, pp.4142-4149*, 2001
80. **B. S. Shelton, T. G. Zhu, M. M. Wong, H. K. Kwon, C. J. Eiting, D. J. H. Lambert, S. P. Turini, and R. D. Dupuis, "**Ultrasmooth GaN Etched Surfaces Using Photoelectrochemical Wet Etching and Ultrasonic Treatment", *Electrochemical and Solid-State Letters, No.3, pp.87-89,* 2002
81. **J. M. Hwang, J. T. Hsieh and H. L. Hwang, and W. H. Hung,** " A damaged reduced process revealed by photoluminescence in photoelectrochemical etching GaN", *TaiWan,* 1999
82. **Y. Liu, J. A. Bardwell, S. P. McAlister, H. Tang, J. B. Webb, and T. W. MacElwee,** "Bias Stress Measurements on High Performance AlGaN/GaN HFET Devices", *Phys. Stat. Sol. (a) 188, No.1, pp.233-237,* 2001
83. **W. K. Fong, S. W. Ng, B. H. Leung, and C. Surya, "**Characterization of low-frequency noise in molecular beam epitaxy-grown GaN epilayers deposited on double buffer layers", *J. Appl. Phys. Vol.94, No.1, pp.387-391*, 2003
84. **R. Oberhuber, G. Zandler, and P. Vogl, "**Mobility of two-dimensional electrons in AlGaN/GaN modulation-doped field-effect transistors", *Appl. Phys. Lett. Vol.73, No.6, pp.818-820,* 1998

85. **S. K. Jha, B. H. Leung, C. Surya, H. Schweizer, and M. H. Pilkhuhn,** "Studies of hot-electron degradation in GaN HEMTs with varying gate recess depths", *Proc. of SPIE Vol.5844, accepted*
86. **J. A. Garrido, F. Calle, E. Munoz, I. Izpura, J. L. Sanchez-Rojas, R. Li, and K. L. Wang, "**Low-frequency noise and screening effects in AlGaN/GaN HEMTs", *Electron. Lett. Vol.34, 2357,* 1998
87. **A. Balandin, S. V. Morozov, S. Cai, R. Li, K. L. Wang, G. Wijeratne, and C. R. Viswanathan, "**Low flicker-noise GaN/AlGaN heterostructure field-effect transistors for microwave communications", *IEEE Trans. Microwave Theory & Tech. Vol.47, No.8, 1413,* 1999
88. **S. L. Rumyantsev, M.E. Levinshtein, R. Gaska, M.S. Shur, J. W. Yang, and M. A. Khan, "**Low-frequency noise in AlGaN/GaN heterojunction field effect transistors on SiC and sapphire substrate", *J. Appl. Phys. Vol. 87,No.4, 1849-1855,* 2000
89. **S. A. Vitusevich, S. V. Danylyuk, N. Klein, M. V. Petrychuk, V. N. Sokolov, V. A. Kochelap, A. E. Belyaev, V. Tilak, J. Smart, A. Vertiatchikh, and L. F. Eastman, "**Excess low-frequency noise in AlGaN/GaN-based high-electron-mobility transistors", *Appl. Phys. Lett. Vol.80, No.12, pp.2126-2128,* 2002
90. **A. van der Ziel, "***Noise in Solid State Devices and Circuits***",** *New York: Wiley, pp.296-297*, 1986
91. **S. L. Rumyantsev, N. Pala, M.S. Shur, E. Borovitskaya, A. P. Dmitriev, M.E. Levinshtein, R. Gaska, M. A. Khan, J. W. Yang, X. H. Hu and G. Simin, "**Generation-Recombination Noise in GaN/AlGaN Heterostructure Field Effect Transistors", *IEEE transactions on electron devices, Vol.48, No.3, pp.530-534,* 2001
92. " Generation-recombination noise in AlGaN/GaN heterostructure field effect transistors", *Proc. of SPIE Vol.5113, pp.221-226*

93. **C. P. Chan, W. K. Fong, P. K. Lai, Y. H. Loke, C. Surya, T. M. Yue, H. C. Man, X. Xiu and R. Zhang, "**Low-frequency excess noise characterizations of laser-assisted debonded GaN films", *Applied Surface Science, accepted*
94. **J.Q. Xie, W.K. Fong, B.H. Leung, C.F. Zhu, and C. Surya,** "Study of Low-frequency excess noise in Ga-polarity GaN epitaxial layers", *Fluctuation and Noise Letters, Vol.1, No.4, pp.R163-R174,* 2001
95. **A. Kuliev, V. Kumar, R. Schwindt, D. Selvanathan, A.M. Dabiran, P. Chow and I. Adesida,** "0.15µm gate-length AlGaN/GaN HEMTs with varying gate recess length", *Solid-State Electronics, Vol.47,* 117-122, 2002
96. **Jae-Seung Lee, Jong-wook Kim, Doo-Chan Jung, Chang-Seok Kim, Won-Sang Lee, Jae- Hak Lee, Jin-Ho Shin, Moo-Whan Shin, Jae- Eung Oh and Jung-Hee Lee, "**Photo-Electrochemical Gate Recess Etching for the Fabrication of AlGaN/GaN Heterostructure Field Effect Transistor", *J. Appl. Phys. Vol.* 40, L198-L200, 2001
97. **Jong-wook Kim, Jae-Seung Lee, Won-Sang Lee, Jin-Ho Shin, Doo-Chan Jung, Moo-Whan Shin, Chang-Seok Kim, Jae- Eung Oh, Jung-Hee Lee and Sung-Hee Lee, "**Microwave performance of recessed gate $Al_{0.2}Ga_{0.8}N$ HFETs fabricated using a photoelectrochemical etching technique", *Materials Science and Engineering* B95, 73-76, 2002